UCRL-9682

UNIVERSITY OF CALIFORNIA
Lawrence Radiation Laboratory
Berkeley, California

Contract No. W-7405-eng-48

MACROSCOPIC INSTABILITY OF THE POSITIVE COLUMN IN A MAGNETIC FIELD

George A. Paulikas and Robert V. Pyle

April 27, 1961

DISCLAIMER

MACROSCOPIC INSTABILITY OF THE POSITIVE COLUMN IN A MAGNETIC FIELD

George A. Paulikas and Robert V. Pyle

Lawrence Radiation Laboratory
University of California
Berkeley, California

April 27, 1961

ABSTRACT

The positive column of a glow discharge has been shown to become hydromagnetically unstable when immersed in a longitudinal magnetic field of the order of 1 kgauss. The instability transforms the azimuthally symmetric column into a constricted, rotating, helical state; neither this new steady state nor its properties are predicted by classical theories. The occurrence of this instability explains the previously mysterious "anamoleus diffusion" observed by Lehnert.

The properties of the helical state have been measured in H_2, D_2, He, and Ne as function of gas pressure and tube radius. The dependence of the critical magnetic field, and the frequency and wavelength of the oscillation on the kind of gas, pressure, and the tube radius are in fairly good agreement with the predictions of the perturbation theory of Kadomtsev and Nedospasov. The onset of the instability is also fairly well predicted by the sheath-instability theory of Hoh, but the agreement is not as good as in the previous case, nor is the nature or appearance of the instability specified.

MACROSCOPIC INSTABILITY OF THE POSITIVE COLUMN† IN A MAGNETIC FIELD

George A. Paulikas* and Robert V. Pyle

Lawrence Radiation Laboratory
University of California
Berkeley, California

April 27, 1961

I. INTRODUCTION

The positive column of a low-pressure glow discharge contains a constant longitudinal electric field and a slowly varying radial field, with $n_+ \approx n_- = n$. Electron densities are typically of the order of 10^9 to 10^{11} per cm^3. Electron temperatures correspond to several electron volts, and ion temperatures are approximately the same as the temperatures of the neutral gases.[1] The early experiments concerning the behavior of such a plasma in a longitudinal magnetic field,[2,3,4] although limited by the rather low available magnetic fields and complicated by end effects, were found to give results consistent with the theories of Tonks,[5] Langmuir and Tonks,[6] and Schottky.[7] Bickerton and von Engel reinvestigated the positive column

---

*National Science Foundation Fellow.

†This work was done under the auspices of the U. S. Atomic Energy Commission.

1. G. Francis, in Handbuch Der Physik, Vol. 22, ed. by S. Flugge (Springer-Verlag, Berlin, 1956).
2. C. S. Cummings and L. Tonks, Phys. Rev. 59, 517 (1941).
3. G. N. Rohklin, J. Phys. (USSR), 1, 347 (1939).
4. E. Reichrudel and G. Spivak, J. Phys. (USSR), 4, 211 (1941).
5. L. Tonks, Phys. Rev. 56, 360 (1939).
6. L. Tonks and I. Langmuir, Phys. Rev. 34, 876 (1929).
7. W. Schottky, Physik. Z. 25, 342 (1924).

in a magnetic field with a geometry which avoided some of the complicating end effects.[8] Their measurements of the electric fields, as well as the charged-particle distribution in longitudinal magnetic fields up to 600 gauss, were also in good agreement with the classical theories. Their work has been extended to considerably stronger magnetic fields by Lehnert[9] and Hoh and Lehnert,[10] whose measurements of the longitudinal electric field as a function of the applied magnetic field showed that above some critical magnetic field B_c the losses of particles no longer decrease with increasing magnetic field--as predicted by theory--but, instead, increase with increasing magnetic field.

Lehnert's results revived interest in the possibility that enhanced diffusion is caused by electrical oscillations in the plasma, as suggested by Bohm.[11] Our work was an effort to understand the nature of the instability and the origin of the increased losses.

---

8. R. J. Bickerton and A. von Engel, Proc. Phys. Soc. (London), B69, 468 (1956).
9. B. Lehnert, in Proceedings of the Second United Nations International Conference on the Peaceful Uses of Atomic Energy, Vol. 32 (United Nations, Geneva, 1958), p. 349.
10. F. C. Hoh and B. Lehnert, Phys. Fluids 3, 600 (1960).
11. D. Bohm, E. H. S. Burhop, H. S. W. Massey, and R. M. Williams, in The Characteristics of Electrical Discharges in Magnetic Fields, ed. by A. Guthrie and R. K. Wakerling (McGraw-Hill, New York 1949).

It has been shown that at B_c a macroscopic instability appears in the column, the observed increase in particle losses being associated with the formation of a new azimuthally asymmetric steady state.[12,13] The results of an experimental investigation of the development and properties of this anomalous steady state of the positive column are presented herein and compared with the theories of Hoh[14] and Kadomtsev and Nedospasov.[15]

II. THEORY OF THE POSITIVE COLUMN IN A LONGITUDINAL MAGNETIC FIELD

A. The Classical Theory

The symbols listed below are used in the discussion which follows.

B	Magnetic field.
D_a	Ambipolar diffusion coefficient at field B.
$D_{\mp}$	Diffusion coefficients of electrons or ions.
E_z	Axial electric field.
$\Gamma_{\mp r}$	Radial particle flux of electrons or ions.
J_0, J_1	Bessel functions of order zero, order one.
$\vec{j}$	Electric-current density.

---

12. T. K. Allen, G. A. Paulikas, and R. V. Pyle, Instability of the Positive Column in a Magnetic Field, Phys. Rev. Letters, 5, 409 (1960), and Lawrence Radiation Laboratory Report UCRL-9110, same title, (unpublished) (1960).
13. G. A. Paulikas, The Positive Column in a Longitudinal Magnetic Field (Ph. D. Thesis), Lawrence Radiation Laboratory Report UCRL-9588, February 27, 1961 (unpublished).
14. F. C. Hoh, Phys. Rev. Letters 4, 559 (1960).
15. B. B. Kadomtsev and A. V. Nedospasov, J. Nuclear Energy, Part C, 1, 230 (1960).

κ	Boltzmann constant.
$k = \frac{2\pi}{\lambda}$	Wave number.
$\Lambda_{\pm}$	Mean free path of ions or electrons.
λ	Wavelength.
$\mu_{\mp}$	Electron or ion mobilities.
$m_{\mp}$	Electron or ion masses.
$n_{\mp}$, n	Particle densities of electrons or ions
ν_i	Number of ionizations per second per electron.
$\Omega_{\mp}$	Electron or ion cyclotron frequencies.
p	Neutral gas pressure (reduced to $0^{\circ}C$).
R	Discharge-tube radius.
$T_{\mp}$	Electron or ion temperature.
$\tau_{\mp}$	Mean time between collisions of electron or ion with neutral particle.
U(r)	Radial potential distribution.
$v_{\mp}$, $v_{+r,z}$	Electron or ion drift velocities and components.
v_+	Ion thermal velocity.

The particle losses in the presence of a longitudinal magnetic field B are described by the ambipolar diffusion coefficient.[16]

$$D_a(B) = \frac{D_+\mu_- + D_-\mu_+}{\mu_+ + \mu_-} \cdot \frac{1}{1 + \mu_+\mu_- B^2}, \qquad \text{(II-1)}$$

where $D_{\pm}$, $\mu_{\pm}$ are the diffusion coefficients and mobilities at $B = 0$.

---

16. W. P. Allis and S. J. Buchsbaum, Notes on Plasma Dynamics, Summer Program, MIT (1959).

Volume recombination is neglected; however, Pahl has shown that the inclusion of this loss mechanism does not materially affect the behavior of the column.[17] In the noble gases, as well as in hydrogen and deuterium, it is also permissible to neglect electron attachment. With these simplifying assumptions, the particle balance is described by

$$\nabla^2 n(\vec{r}) + (\nu_i / D_a)\, n(\vec{r}) = 0, \qquad \text{(II-2)}$$

where ν_i is the number of ion pairs produced per second per electron. In a long cylindrical geometry, provided ν_i is independent of n, the solution of Eq. (II-2) is

$$n(r) = n(0)\, J_0 \left(\sqrt{\nu_i / D_a}\; r \right), \qquad \text{(II-3)}$$

where r is the radial coordinate. From the boundary conditions one can then obtain expressions relating the ionization rate and hence the electron temperature T_- to the parameters of the discharge for the two pressure regions of interest,[8] described by the average mean free path Λ:

$$\nu_i = (2.4/R)^2\, D_a \quad \text{for } \Lambda \ll R, \qquad \text{(II-4a)}$$

and

$$\frac{4 D_a}{R v_+} = \frac{1\, J_0(x)}{x\, J_1(x)}, \qquad x = \left(\frac{\nu_i}{D_a} \right)^{1/2} R \quad \text{for } \Lambda \approx R. \qquad \text{(II-4b)}$$

The form of $\nu_i(T_-)$ depends strongly upon the behavior of the ionization cross section near threshold as well as upon assumptions of the shape of the electron-velocity distribution, which is not necessarily Maxwellian. Measurements of the electron-velocity distribution in a discharge with standing striations show

---

17. M. Pahl, Z. Naturforsch. 12a, 632 (1957).

that a distinct high-energy group is present.[18] Since the usual "uniform" column commonly contains moving striations,[19] a similar high-energy group may be present and contribute significantly to ν_i.

Either of Eqs. (II-4) may be solved for T_- as a function of the magnetic field for a given pressure and radius, although an additional assumption regarding ion temperatures is necessary for solution of (II-4b). If quadratic ionization processes are included--i.e., ionizations from excited atomic states--the plasma-balance equations cannot be reduced to the simple form of Eqs. (II-4); the result of this modification is to depress electron temperature slightly.[20]

The longitudinal electric field is determined by the power input required to maintain the electron distribution at a temperature T_- determined from Eqs. (II-4). If $X(T_-)$ denotes the fractional energy lost by an electron in a collision, including elastic, inelastic, and wall losses, the electric field is found to be

$$E_z = \left(\frac{64}{\pi}\right)^{1/4} \cdot \left[X(T_-)\right]^{1/2} \cdot \frac{\kappa T_-}{\Lambda_- e} \text{ v/cm}, \qquad \text{(II-5)}$$

where Λ_- is the transport mean free path of the electron.[21] The effect of the longitudinal magnetic field will be to decrease the electron temperature, by decreasing particle losses, and this will be reflected in a diminished longitudinal electric field. This has been confirmed experimentally at low magnetic fields

---

18. R. L. F. Boyd and N. D. Twiddy, Proc. Roy. Soc. (London) A250, 53 (1959).
19. T. Donahue and G. H. Dieke, Phys. Rev. 81, 248 (1951).
20. E. Spenke, Z. Physik 127, 221 (1950).
21. A. von Engel, Ionized Gases (Oxford University Press, 1955).

by the experiment of Bickerton and von Engel.[8] A departure from the monotonic decrease of E_z with increasing B, such as found by Lehnert and Hoh at fields in the kilogauss range, may consequently be taken as an indication of a change in the particle loss.[9,10] (Ecker has pointed out, however, that the longitudinal electric field is a rather insensitive measure of the particle loss; large changes in the diffusion coefficient near the wall are required to alter E_z noticeably.[22])

The radial potential distribution in a cylindrical column, if one assumes ambipolar diffusion and neglects ion-electron interactions, is found from the equation of motion to be

$$\frac{eU(r)}{kT_-} = \frac{1 + \mu_+\mu_- B^2 \left[(\mu_+/\mu_-) - (T_+/T_-) \right]}{1 + \mu_+\mu_- B^2} \ln \left[J_0 \left(\frac{2.4r}{R} \right) \right], \qquad (11\text{-}6)$$

which exhibits a monotonic increase or decrease with radius depending on the relations between μ_+, μ_-, T_+, and T. The reduction of the radial potential variation with increasing magnetic field as predicted by Eq. (11-6) has previously been confirmed experimentally, except for curious asymmetries in the results, probably due to the perturbing effects of the probes used in the measurements. We also have confirmed and extended this result in a search for micro-instabilities, the results of which will be reported elsewhere. The measurements were consistent with the assumption of ambipolar diffusion.

B. Analyses of Stability

Recently Hoh[14] and Kadomtsev and Nedospasov[15] have theoretically investigated the stability of the positive column from two differing standpoints. Hoh starts with the criterion, due to Bohm, for the stability of the sheath surrounding the plasma.[11] The radial ion velocity at the sheath must satisfy

---

22. G. Ecker, Phys. Fluids 4, 127 (1961).

$$v'_{+r} \geq (\kappa T_- / m_+)^{1/2} , \qquad \text{(II-7)}$$

where T_- is the electron temperature and m_+ is the ionic mass. By considering the effect of the magnetic field upon the radial drift velocity of the ions, he is able to show that Eq. (II-7) is not satisfied for magnetic fields

$$B \geq B_c = (\mu_{+1}\,\mu_{-1})^{1/2}\ (2.4\ \frac{g'}{R}\ p - p^2)^{1/2}, \qquad \text{(II.8)}$$

where

$$g' = (\kappa m_+ / T_-)^{1/2}\ \frac{T_+ + T_-}{e} \cdot \frac{\mu_{+1}\mu_{-1}}{\mu_{+1} + \mu_{-1}} \cdot \frac{J_1(2.4r'/R)}{J_0(2.4r'/R)} . \qquad \text{(II-9)}$$

Here $\mu_{\pm 1}$ are the mobilities at 1 mm Hg and p is the neutral gas pressure. The primed quantities are to be evaluated at the sheath edge, a circumstance which introduces some uncertainty into the value of g'.

Hoh postulates that when Bohm's criterion is not satisfied, an instability of the sheath develops which then transports charged particles across the field at a rate in excess of ordinary collisional diffusion. The mechanism by which such a possible sheath instability develops to affect the macroscopic behavior of the plasma is not discussed. The expression for B_c (Eq. II-8) is quite sensitive to assumptions regarding the ionic species, but depends relatively weakly on the electron temperature T_-. Hall has criticized this approach to stability considerations by pointing out that Bohm's criterion is not applicable in the case of the positive column, as the potential drop across the sheath is only of the order of a few $\kappa T_- / e$.[23] The nonsatisfaction of Bohm's criterion therefore should be interpreted as an argument to re-examine and modify the

---

23. L. S. Hall, On the Application of Bohm's Criterion for the Formation of a Sheath, Phys. Fluids (Letter) 4, 388 (1961).

model used in the derivation of Eq. (II-7), rather than an indication of a true instability.

Kadomtsev and Nedospasov approach the stability problem by a perturbation analysis of the positive column. Their treatment is focused upon a region of the magnetic fields where $\Omega_- \tau_- \gg 1$ and $\Omega_+ \tau_+ \ll 1$, where $\Omega_\pm$, $\tau_\pm$ are the ion and electron cyclotron frequencies and the mean times between collisions with neutrals. Such an approximation is quite valid, for our experimental conditions, in the vicinity of the critical magnetic field. Further, it is assumed that the conditions in the unperturbed state are governed by ambipolar diffusion and single-stage ionization; two-step processes and end effects are neglected.

Perturbation of the form

$$n(\vec{r},t) = n_0 J_0 (2.4/R) + n_1 J_1 (3.83r/R) \exp [i(m\Phi + kz - \omega t)] \qquad \text{(II-10)}$$

are now introduced into the equations of motion and continuity:

$$\frac{\kappa T_\mp}{m_\mp n} \nabla n = \mp \frac{e}{m_\mp} \vec{v}_\mp \times \vec{B} \pm \frac{e}{m_\mp} \nabla U - \frac{\vec{v}_\mp}{\tau_\mp},$$

$$\frac{\partial n}{\partial t} + \nabla (n \vec{v}_+) = \frac{\partial n}{\partial t} + \nabla (n \vec{v}_-) = \nu_i n . \qquad \text{(II-11)}$$

When Eq. (II-10) and its equivalent for $U(\vec{r})$ are substituted into Eqs. (II-11), a dispersion relation giving ω as a function of k is obtained. From the condition that $\mathrm{Im}(\omega) < 0$, the requirements for stability under such a perturbation can then be determined. The behavior of Eqs. (II-11) under perturbations of general form $n_1(r)$, $U_1(r)$ is not discussed. The choice of the form of the perturbation, $J_1(3.83r/R)$, is arbitrary; the effect of the second term on the right Eq. (II-11) is to introduce an asymmetry into the density distribution.

The qualitative physical picture thus consists of studying the time dependence of perturbations in the plasma. When there is no magnetic field or the magnetic field is weak, the disturbance in the particle density will soon disappear because of a rapid diffusion of particles from the region of high charge density. In a sufficiently strong magnetic field, however, the radial diffusion will be retarded and a perturbation will persist long enough that $j \times B$ forces can cause the initial disturbance to grow.

For stability, therefore,

$$\mathrm{Im}(\omega) = \left(\frac{3.83}{R}\right)^2 \frac{D_-}{y(\Omega_-\tau_-)^2} \left[\left(\frac{0.33}{\Omega_-\tau_-}\, m\frac{\mu_-}{\mu_+}\right)^2 + \left(\frac{1+y}{y} + \frac{k^2}{0.79}\frac{\mu_-}{\mu_+}\frac{R}{3.83}\right)^2\right]$$

$$\left[-\frac{(1.28+y)}{0.8(y+1)}x^4 - (2+y)x^2 - 0.12\frac{\mu_-}{\mu_+}\frac{ym^2}{y+1} - 0.6(1+y) + 0.2xyv^*\frac{\mu_-}{\mu_+}\right] < 0\,, \qquad \text{(II-12)}$$

where

$$x = \frac{k\Omega_-\tau_- R}{3.83}\,,\quad v^* = \frac{v_{-z}R}{2.4D_-}\,,\quad \text{and}\quad y = \frac{\mu_+}{\mu_-}(\Omega_-\tau_-)^2\,.$$

Since the sign of Eq. (II-12) depends only on the terms in braces, the conditions for stability can be simplified to

$$Kx^4 + Fx^2 + G > 0.16\, mv^* x\,(\mu_-/\mu_+)\,, \qquad \text{(II-13)}$$

where

$$K = \frac{1.28+y}{y(y+1)}\,;\quad F = \frac{0.8(y+2)}{y}\,;\quad G = \frac{0.48(1+y)}{y} + 0.1\,\frac{\mu_-}{\mu_+}\,\frac{m^2}{1+y}\,.$$

Hence, only for $m > 0$ will the plasma be unstable. Note also that an electron drift velocity v_{-z} is necessary. A current is required, but its magnitude does not affect the calculations of the characteristics of the instability.

The form of Eq. (II-12) is presented in Fig. 1. Since at B_c, $\partial \mathrm{Im}(\omega)/\partial k = 0$ as well as $\mathrm{Im}(\omega) = 0$, Eq. (II-13) can be reduced to an expression independent of k:

$$x^2 = \frac{-F + (F^2 + 12KG)^{1/2}}{6K}; \quad 0.08 v^* = \frac{\mu_+}{m\mu_-} \left(2Kx^2 + F\right) x. \qquad \text{(II-14)}$$

Eq. (II-14) can then be solved for B_c in terms of the parameters of the discharge.

In the presence of azimuthal density gradients and an azimuthal electric field, the radial particle flux takes the form[16]

$$\Gamma_{+r} = \Gamma_{-r} = - \frac{D_a(0)}{1+\mu_+\mu_- B^2} \frac{\partial n}{\partial r} + \frac{\mu_+\mu_- B}{1+\mu_+\mu_- B^2} \left\{ nE_\phi + \frac{1}{\mu_+ + \mu_-} \frac{1}{r} \frac{\partial}{\partial \phi} \left[(D_- - D_+) n \right] \right\}. \qquad \text{(II-18)}$$

When averaged over time, the oscillations of density and potential contribute to $\Gamma_{\pm r}$ and thus give rise to an increased effective mobility across the magnetic field. The anomalous losses are then reflected in an increase of the longitudinal electric field for constant current.

III. APPARATUS AND PROCEDURE

Two independent experimental arrangements were employed for this work. The layout of the primary system is shown in Fig. 2. In order to minimize the possibility of the end effects, a tube geometry of large length-to-radius ratio was used. The criterion developed by Simon[24] for the transverse diffusion to be ambipolar in a plasma column of radius R and immersed in a magnetic field of length L is

$$L/R > (q/R)^{1/2} \Omega_- \tau_-, \qquad \text{(III-1)}$$

where $1/q = 1/n \; dn/dr$, n is the electron density, Ω_- is the electron cyclotron frequency, and τ_- the electron-neutral collision time. For example, in a

---

24. A. Simon, Phys. Rev. 98, 317 (1955).

column of helium at a pressure of 0.1 mm Hg, with R = 3 cm, L = 200 cm, and $q/R \approx 1/2$, the magnetic field must be less than 1000 gauss in order for the plasma to be free from end effects. Similar results are obtained for other gases, and the above criterion is satisfied for most of the present operating conditions. "Simon" diffusion should leave the potential distribution essentially unaffected by the magnetic field. Our radial potential measurements have not shown any significant deviation from the predictions of ambipolar diffusion, even in cases where the Simon criterion (Eq. III-1) is clearly not satisfied. This suggests that in a glow discharge, measurements are more likely to be confused by too short a positive column at low pressures than by nonambipolar diffusion.[25]

Discharges in pyrex tubes 300 cm long and 0.9, 1.27, and 2.75 cm in radius were studied. Both electrodes were attached to the main body of the tube by ground glass joints and sealed with Apiezon wax. Such an arrangement permitted a number of types of electrodes and configurations to be employed interchangeably. Discharge currents from 50 to 500 ma dc were drawn from a hot tungsten cathode, although a dispenser-type cathode was also used for some measurements. These currents were obtained from an electronically regulated power supply. A rectangular current pulse up to 10 amp high, up to 10 msec long, and with a variable repetition rate, drawn from a small capacitor bank, permitted transient study of discharges at considerably higher particle densities.

The magnetic field was provided by ten 9-in. i.d. water-cooled coils 6 in. wide and spaced 2-1/4 in. apart. The axial field, measured by a flip coil, varied by ±3% at a radius of 4cm because of the spaced coils. Field strengths (dc) up to 7 kgauss were used. To study the time-resolved behaviour of the plasma, the magnet could be pulsed up to 1 kgauss by a small condenser

---

25. See, however, C. Ekman, F.C. Hoh, and B. Lehnert, Phys. Fluids 3, 833 (1960).

bank, the field rising sinusoidally to a maximum in 10 msec.

The discharge tubes were aligned with the magnetic field by visually following the progress of a number of low-pressure discharges in a tube of larger diameter. Well-defined beams traveled from a cathode, which consisted of an array of tungsten points placed at a radius slightly smaller than the radius of the discharge tube, to an anode almost filling the tube.[26] The effects of the radial components of the field caused by the gaps between magnet coils were not visible to the eye. The radial field components should cause a line of force to be shifted by about 0.5 mm at $r = 2$ cm as it travels from the center of a coil to the center of a gap; 0.5 mm is comparable to the tolerence on the tube radius.

Langmuir-type probes were spaced along the tube in order to obtain measurements of the longitudinal electric fields. The probes were made of glass-coated 0.5-mm tungsten rod, ground flat at one end and protruding 3 to 5 mm from the tube wall. Midway between the electrodes, Langmuir probes of various shapes and types could be introduced into the tube and moved along a diameter by means of a micrometer screw.

The gaps between the coils of the magnet, together with a periscopic arrangement of front-surface mirrors, permitted a number of well-collimated magnetically shielded photomultipliers to view the discharge tube along its entire length. Signals were displayed on Tektronix-551 or -555 oscilloscopes and photographically recorded. A rotating-mirror streak camera yielded space-and-time-resolved data on the light fluctuations in the tube. The space resolution could be extended to two dimensions through the arrangement shown in Fig. 3. Because of the limited light intensity, 100 μsec/cm was the maximum useful writing speed, when Polaroid 3000 film was used. In discharges of low light

---

26. A. W. DeSilva and J. M. Wilcox, Rev. Sci. Instr. 31, 455 (1960).

intensities, such as argon, a bank of photomultipliers (Fig. 3) substituted effectively for the streak camera. This device also permitted detailed examination of short time intervals during the growth of the instability.

The electrical signals associated with the plasma were frequency-analyzed by using a series of radio detectors covering the frequency range from 5 kc to 250 Mc, and 1 to 10 kMc.[27] The detectors were coupled to the plasma either through wall probes or through capacitative pickups outside the tube.

When the plasma density could be made sufficiently high, an 8-mm microwave interferometer was used to study the behavior of the electron density. Densities as low as $5\times10^{10}/cm^3$ could be measured.

An oil diffusion pump with a refrigerated baffle system and a trap kept at liquid nitrogen temperature gave the system a base pressure of the order of 10^{-7} mm Hg. During the experimental runs, gases were continuously bled through the system. Other methods of gas handling were used, such as the introduction of a charcoal trap kept at liquid nitrogen temperature, but with no effect on the experimental results.

All measurements with a varying magnetic field were taken at constant current, data being recorded on an x-y or strip-chart recorder.

The experimental arrangement of the secondary system is shown in Fig. 4. The purpose of this subsidiary experiment was to study the behavior of the column in a short-tube geometry. The diagnostic tools described in the previous sections could be readily transferred to this system. The vacuum was of comparable quality; however, a mercury diffusion pump was used here.

---

27. We are grateful to the U. S. Navy installation at Vallejo for loan of this equipment.

IV. RESULTS

A. The Longitudinal Electric Field and the Critical Magnetic Field

We have investigated the behavior of the longitudinal electric fields, measured between wall probes, in tubes of 0.9, 1.27, and 2.75 cm radius, using discharges of hydrogen, deuterium, helium, neon, and argon. Typical experimental measurements of the fields as functions of the applied magnetic field at constant discharge currents are presented in Figs. 5 and 6. (A more complete set of data is given in Ref. 13.) In agreement with the experiments of Lehnert and Hoh,[10] we find that the axial electric field decreases with increasing magnetic field up to some critical field B_c. At B_c the slope of E_z -vs-B curve changes sign. In general, E_z increases with increasing B above B_c, although in some regimes of pressures, gas, and tube radius, further undulations of the curve may occur. (The exact form of the curves at pressures below about 0.2 mm Hg depends slightly upon whether the magnetic field was increased or decreased during a run.)

The shapes of the curves and the values of B_c were not affected by varying electrode materials and geometries or external circuit parameters. Modest misalignment of the discharge tubes with respect to the axis of the magnetic field changed the shapes of the E_v-vs-B curves above B_c but did not change the value of B_c. Placing one or both electrodes inside the magnetic field left B_c unchanged except at rather low pressures (Fig. 7). A series of measurements taken in the "short tube" system (Fig. 4) yielded results consistent with the curves from the primary system (tube 300 cm long), again with the exception of low pressures. The deviations observed at low pressures in short-tube geometries are probably caused by the shortening of the positive column at low pressures and the encroachment of the Faraday dark space into the region of measurement.

We have calculated the longitudinal electric field (Eq. II-5) as a function of the magnetic field for several sets of typical discharge parameters, and find good qualitative agreement between theory and experiment up to B_c. At higher magnetic fields the experimental curves deviate markedly from the theoretical calculations; specifically, the classical theory of the positive column does not predict any deviation from the monotonic decrease of the axial electric field with increasing applied magnetic field.

Optical observations of the light from the discharge by means of photomultipliers and a stereo streak camera have shown that at B_c the column loses its azimuthal symmetry and becomes a constricted, rotating, luminous helix (Fig. 18, a, b). We defer until a later section detailed discussion of the properties of this phenomenon; we find that the apparently enhanced diffusion from the column, characterized by a longitudinal field considerably in excess of theoretical predictions, is the result of an instability which develops at B_c and transforms the uniform column into a constricted helical column.

The behavior of B_c as a function of gas, gas pressure (reduced to 0° C), and tube radius is presented in Figs. 8 through 16, together with the B_c-vs-p curves calculated from the theories of Hoh[20] and Kadomtsev and Nedospasov.[15] The experimental points represent results obtained over a period of months with a variety of tubes of a given radius and various methods of gas handling. Preceding any set of measurements, the discharges were repeatedly flushed and allowed to run for 2 to 6 hours until no significant impurity lines sere detectable spectroscopically. However, we have no quantitative information on the impurities present. Appreciable admixtures of impurities (99% He, 1% A; 99% A, 1% N_2) yielded E_z -vs-B curves from which it was impossible to deduce a critical field.

The scatter of the experimental points is probably the result of several effects: (a) in an unbaked system such as ours the impurity level is certainly not constant over long periods of time; (b) the magnetic field could be determined from the x-y recorder to ±2%; and finally, (c) at high pressures the determination of B_c was difficult because of the very gradual transition to the anomolous state.

An IBM 650 was used to solve Eq. (II-14) with m = 1 (theory of Kadomtsev and Nedospasov) by successive approximations. Here we have used the experimentally determined longitudinal electric field at the critical magnetic field as an input parameter. The electron temperature was calculated from the modified Schottky theory,[8] assuming $T_+ = 400^\circ$ K. A calculation with $T_+ = 1000^\circ$ K is shown in Fig. 10 to illustrate the dependence of B_c on the ion temperature. In calculating the values of B_c as predicted by the sheath-instability theory, we have assumed, with Hoh,[14] $T_-/V_i = 1200^\circ$ K/volt and $J_0(2.4r'/R) = 0.013$. Atomic data from the compilation by Brown[28] were used; the value for the mobility of H_2^+ was taken from the work by Chanin.[29]

Considerable uncertainty exists as to the actual conditions in the positive column, e.g., both atomic and molecular ions are known to be present.[30] Since the theory of Hoh, although depending weakly on T_-, is particularly sensitive to assumptions regarding the ion species, we have calculated and plotted curves for the two limiting compositions. The theory of Kadomtsev and Nedospasov, on the other hand, is relatively insensitive to

---

28. S. C. Brown, Basic Data of Plasma Physics (John Wiley and Sons, New York, 1959).

29. L. M. Chanin (Honeywell Research Center), private communication.

30. M. Pahl, Z. Naturforsch. 14a, 239 (1959).

changes in the ion mobility. Here the assumption that only molecular ions are present at a given pressure decreases the calculated critical magnetic field slightly below the value obtained by using atomic ion mobilities (Figs. 13 through 16). However, the electron temperature T_- enters these calculations in an important way; for a given pressure B_c varies roughly as T_-. The effect of the moving striations on T_- is not known; we find, however, that the experimental B_c -vs-p curve passes smoothly from the striated to the unstriated regime. Values of the electron temperature, as determined from Langmuir-probe measurements, Fig. 17, were also in reasonable agreement with theoretical calculations, at least up to B_c. Above B_c the experimental results are of doubtful value. The apparent electron temperature increases with increasing particle losses. In addition, the marked oscillations of the current channel result in oscillations of the potential of the plasma about some average value at the probe. Because of the nonlinearity of the probe characteristics, the potential oscillations create an average probe characteristic which indicates an apparently higher electron temperature.

The value of B_c increases slowly with increasing discharge current (Figs. 7, 8, and 14). The effect is more pronounced at relatively high pressures (Fig. 11). At high current densities and at pressures above a few millimeters, an appreciable fraction of the ionizations may occur from excited atomic levels, especially if long-lived metastable states are present,[20] with a consequent decrease of the longitudinal electric field. This in turn, according to the K and N theory, will result in a higher B_c. As shown in Fig. 11, there is qualitative agreement between this theory and experiment.

At high values of the pressure-radius product pR, the positive column constricts into a filament of current; Fowler finds that appreciable constriction

is present in helium discharges with $pR \approx 10$ cm/mm Hg.[31] The causes of pressure constriction are not well understood; it is not predicted by the Schottky theory. It has been suggested that the constriction of the positive column comes about as a consequence of a rapid decrease of electron temperature with increasing pressure and a subsequent piling up of the electrons in the center of the discharge.[32] A temperature lower than predicted by the Schottky theory would decrease our theoretical B_c values at a given pressure, as calculated from the theories of Hoh, and Kadomtsev and Nedospasov. The decrease of the experimental helium B_c-vs-p curves starting at $pR \approx 4$ may thus be connected with the beginning of pressure constriction in the column; a similar argument may also apply to other gases.

B. Properties of Instability

The striking optical behavior of the column at the critical magnetic field has already been mentioned briefly. Luminous helices of the clarity shown in Fig. 18 (a) were observed only for special combinations of gas, pressure, and tube radius. In general the appearance was more chaotic; often moving striations were superimposed on the spirals (as will be shown in Fig. 33a). The transition to the helical state is quite abrupt, and especially so if there are no moving striations present. Thus the presence of moving striations (Fig. 33 b) complicates analysis of the behavior of the column. We have therefore attempted, unsuccessfully, to remove the moving striations

---

31. R. G. Fowler and L. W. Jones, Pressure Constriction in the Positive Column, 13th Annyal Gaseous Electronics Conference, Monterey, California, Oct. 12-15, 1960.

32. R. G. Fowler, Proc. Phys. Soc. (London) B68, 130 (1955).

from the column by adjusting external circuit parameters and by operating an auxiliary discharge at the anode. The latter scheme was meant to provide a source of ions; the oscillations of the anode fall are believed by Pupp to be the source of one species of moving striations.[33] At some discharge conditions, however, we found that the longitudinal magnetic field was able to suppress the striations; a column striated at $B = 0$ can become uniform as the field is raised, and then at B_c makes the transition to the helical mode.

The helical nature of the constriction has been determined by studies with a series of photomultipliers placed along the discharge tube. Wavelengths of the luminous current channel could thus be found by studying the phase differences of the photomultiplier signals. The pitches of the spirals were such that $\vec{J} \times \vec{B}$ was directed toward the tube walls. In Figs. 19 through 23 we show experimental measurements of this wavelength as a function of the neutral pressure.

The perturbation analysis by Kadomtsev and Nedospasov predicts the growth rate of the instability to be a strong function of the wavelength of the instability (Eq. II-12, Fig. 1). Bearing in mind that the above theoretical analysis is based on a small-amplitude theory, whereas our experimental measurements were carried out on the fully developed helix, i.e., a new, azimuthally nonsymmetric steady state, we have computed curves similar to Fig. 1 for the discharge parameters of the experimental points in Figs. 19 through 23. If we assume that the maxima in the $\mathrm{Im}(\omega)$-vs-k curves represent that wavelength that will grow fastest and dominate as the behavior of the column becomes nonlinear, we can arrive at the theoretical values for the instability wavelength. We present these theoretical values ($m = 1$), together with

---

33. W. Pupp, Physik. Z. 34, 756 (1933).

experimental results, in Figs. 19 through 23. Higher values of m shift the maximum of the Im(ω)-vs-k curves toward shorter wavelengths. The agreement between theory and experiment is excellent in the case of helium and satisfactory in the cases of hydrogen, deuterium, and neon. However, even for the latter, the form of the theoretical curves is consistent with experimental results. Measurements in helium could usually be made at magnetic fields not more than 40 gauss above B_c. For H_2, D_2, and Ne it was necessary to raise the magnetic field up to 10 to 20% above B_c in order to find a spiral reasonably free from striation; this may also account for the reversal of experimental and theoretical dependences on ion mass in Fig. 19. During a given measurement the column was monitored with the streak camera and the photomultiplier bank, Fig. 3.

The effect of changes in the length of the magnetic field on the wavelength, is presented in Fig. 24 for several valses of the neutral pressure and the discharge current. We have studied the R = 2.75 cm tube, as here the L/R ratio is most unfavorable. As Fig. 24 indicates, λ approaches an asymptotic value as the length of the magnetic field is increased. The "long tube" approximation becomes increasingly valid with increasing neutral pressures at L/R = 72.

We have attempted to determine the wavelength λ at the earliest possible moment in its development. The small capacitor bank supplying a sinusoidally rising magnetic field was so charged that $B_{max} \approx B_c$; i.e., the magnetic field changed by only a small amount during the time of measurement. The disturbance does not develop simultaneously at all points along the column. The instability is usually seen to arise initially somewhere in the vicinity of the center of the coil, and to propagate in both directions. There is some evidence, however, that at low pressure ($p < 0.1$ mm Hg) the disturbance arises first at the anode end of the magnetic coil.

The dispersion relation derived by Kadomtsev and Nedospasov in considering the stability of the column can also be solved for ω_r, the real frequency of oscillation of the luminous current channel. Under the condition $B \approx B_c$, the expression for ω_r takes the simple form

$$\omega_r \approx \frac{3\mu_+ D_- \beta_1^2}{\mu_-(\Omega_- \tau_-)} (0.6 + x^2), \quad x = \frac{k\Omega_- \tau_-}{\beta_1}, \quad \beta_1 = \frac{3.83}{R} . \qquad \text{(IV-1)}$$

The growth of the instability is driven by $\vec{J} \times \vec{B}$ forces that twist a kink in the current channel into a helix in close contact with the tube walls. From Eqs. (IV-1) and (II-14) we can arrive at an approximate expression for the phase velocity of the perturbation:

$$v_{ph} = \frac{\omega_r}{k} \approx \frac{1.15\, mv_{-z}}{(2F + \sqrt{F^2 + 12KG})} + \frac{68}{R^2} \left(2F + \sqrt{F^2 + 12KG}\right) \left(\frac{\mu_+}{\mu_-}\right)^2 \frac{D_-^2}{mv_{-z}} . \qquad \text{(IV-2)}$$

The second term on the right of Eq. (IV-2) is, for our experimental conditions, usually less than a 30% correction. Typically,

$$\left(2F + \sqrt{F^2 + 12KG}\right) > 3, \text{ thus } v_{ph} < v_{-z} .$$

The luminous helical structure, traveling in the direction of the electron drift, will appear to an observer at some cross section along the tube as a rotating column. This picture has been verified by experimental measurements of the pitch and direction of rotation of the spiral (Fig. 25). In the steady state with $B > B_c$ the luminous column revolves about the tube axis; this rotation is clockwise when the column is viewed in the direction of the magnetic field. In Fig. 26 we present the instantaneous density profile across the column taken with a radially movable Langmuir probe.

The measurements of the frequency of rotation of the luminous current channel are presented in Figs. 27 through 32. The photomultiplier bank, together with the rotating mirror, permitted identification of the spiral mode (under certain conditions the time-resolved light-wave form of axially moving striations is similar to the near-sinusoidal wave form of the azimuthally moving column). Each experimental point in the above figures represent an average of 6 to 12 photomultiplier traces, each trace being about 10 periods long. Again remembering that Eq. (IV-1) was derived by considering small-amplitude disturbances, we have plotted ω_r as a function of pressure with the experimental results shown in Figs. 27 through 32. The observed general decrease of ω with increasing pressure is confirmed theoretically, with good quantitative agreement between experiment and theory for helium.

Measurement of the time development of the wavelength of the instability, as described earlier, also yielded information regarding the changes occurring in the frequency. Using a 400-ma He discharge in a tube of R = 2.75 cm, we obtain the following values for the frequency (rad/sec) at $t \approx 0$ and $t = \infty$:

p (mm Hg)	$t \approx 0$ ($B = B_c$)	$t = \infty$ ($B \approx B_c$)
0.2	5.9×10^4	5.0×10^4
0.37	4.3×10^4	3.8×10^4

As the magnetic field was increased somewhat above B_c, the luminous spiral degenerated into irregular fluctuations of light, Fig. 33 (a). In some cases, this transition was preceded by the appearance of frequencies which modulated ω_r, and abrupt changes in ω_r; sometimes, as in the case of helium, the color of the spiral as seen with the rotating mirror underwent a

change, indicating changes in the electron temperature. We have found that the various transitions just described are intimately connected with the undulations of the E_z-vs-B curves at $B \gg B_c$.

The above discussion suggests that modes higher than m = 1 may be present in the plasma under these circumstances. Indeed, if we calculate B_c-vs-p curves from the theory of Kadomtsev and Nedospasov and let m = 2 (Figs. 10 and 12), we find that the higher mode can appear at fields only slightly higher than B_c. At low pressures we may even have B_c (m = 2) < B_c (m = 1). Experimentally, however, we have been unable to distinguish or identify a symmetric m = 2 mode in the confused state of the plasma above B_c.

The chaotic state of the plasma above the critical magnetic field is reflected in the radial electron-density distribution. The time-average density distribution is noticeably flattened; visually we observed that the luminous column now appears to fill the tube more completely than at B = 0.

We have analyzed the electromagnetic noise generated by the plasma in the frequency ranges 5 kc to 250 Mc and 1 to 10 kMc. in a manner similar to that used by Lehnert. In addition to frequencies associated with moving striations, we find frequencies that correspond to the frequency of the luminous spiral. A broad band of electromagnetic noise from 10 kc to about 2 Mc appears at field slightly above B_c and is associated with the transition from the rather regular spiral mode to a chaotic state of the column, characterized by irregular fluctuations of light. We have not detected any oscillations that could be associated with either cyclotron or plasma frequencies of the electrons or ions.

V. SUMMARY AND CONCLUSIONS

The previously reported anomalous state of the positive column, characterized by a longitudinal electric field that rises with increasing magnetic field, is the result of an instability which appears at B_c, the critical magnetic field. B_c, describing the onset of the instability, varies approximately inversely as the tube radius and directly as the square root of the ion mass. The relatively slow-developing instability results eventually in a steady state in which the plasma density distribution has lost its azimuthal symmetry and formed a long-wavelength rotating spiral. Because of the absence of a net radial current, we believe rotation of the plasma density, as well as of the luminous structure, to be associated with the passing of a potential wave rather than an actual mass motion. The close contact between the luminous current channel and the walls of the tube increases the losses of charged particles and results in an electric field considerably in excess of classical predictions. As the magnetic field is increased to higher and higher values, the behavior of the column becomes increasingly more chaotic, characterized not only by irregular fluctuations of light, but also by a broad band of electromagnetic noise.

We have calculated the onset of the instability from the theories of Kadomtsev and Nedospasov;[15] and Hoh.[14] The shapes of the experimental curves are perhaps more like the calculations from the K and N theory; the rapid decrease of B_c at high pressures as predicted by Hoh is not confirmed by the experimental results in neon and argon. Investigations of B_c at high pressures in helium have shown that B_c is here no longer independent of the discharge current. These findings suggest that both theories may need to be modified to include stepwise ionization and pressure constriction.

The wavelength of the instability as well as its frequency of oscillation is predicted by the theory of K and N. The experimental frequencies and wavelengths were obtained from the fully developed steady-state helix.

It is not obvious that they should be the same as the quantities calculated from a small-amplitude theory. Nevertheless, we find qualitative, and sometimes quantitative, agreement between theory and experiment: the wavelengths decrease with increasing pressure and decreasing radius; the frequencies increase with decreasing radius and decreasing pressure. The inverse relationship between frequency and pressure suggests a connection with the instabilities reported in PIG-type discharges.[34]

We have not been able to unequivocally distinguish between the theory of Hoh and the approach of Kadomtsev and Nedospasov by the critical magnetic field measurements. However, the general agreement between calculation and experiment with regard to wavelength and frequency lends considerable support to the latter theory. The phenomena in the positive column are so complex that anything more than semiquantitative agreement could hardly be expected.

Uncertainties about the ion species present in the discharge permit a latitude in the value of the ion mobility; with a proper choice either theory fits the experimental results reasonably well. Measurements of B_c at high pressures, where the predictions of these theories diverge markedly, may be complicated by pressure constriction. The theory of Hoh, in contrast to the K and N theory, does not require a current for the development of the instability. In principle, a current-free plasma might thus permit a distinction to be made between these theories.

---

34. J. F. Bonnal, G. Briffod, and C. Manus, Compt. rend. 250, 2859 (1960).

ACKNOWLEDGMENTS

We are deeply indebted to Dr. T. K. Allen, who suggested the investigation of the "Lehnert Instability", and was a principal contributor to the discovery of the helical nature of the instability. We wish to thank J. Warren Stearns for helping with the measurements, and Dr. Gunter Ecker, Y. T. Fung, Larry S. Hall, Dr. Wulf B. Kunkel, and Dr. J. Bryan Taylor for valuable discussions of the theory and experiment. We are grateful to Dr. C. M. Van Atta and to Mr. William Baker for supporting this research. The skillful efforts of Harry Powell, John Meneghetti, Louis Biagi and their shops were essential to the success of the experiment. Ferd Voelker and M. C. Horton constructed the microwave gear, and the IBM 650 programs were written by Edna Williams and Elizabeth Meyers.

FIGURE LEGENDS

Fig. 1. The form of Eq. (II-12); $\mathrm{Im}(\omega)$ vs k for several values of B (qualitative).

Fig. 2. The primary experimental arrangement ("long tube" system).

Fig. 3. Schematic of optical diagnostics.

Fig. 4. Secondary, "short tube" system. The anodized-aluminum wire was movable along a diameter for radial potential measurements.

Fig. 5. E_z vs B: He gas, R = 1.27 cm, I = 400 ma.

Fig. 6. E_z vs B: He gas, R = 2.75 cm, I = 400 ma. "Short tube" geometry (Fig. 4).

Fig. 7. B_c vs pressure for various electrode configurations: He gas, R = 2.75 cm. (a) and (d) electrodes outside magnetic field (normal condition); (b) anode in magnetic field; (c) both electrodes in magnetic field; (a), (b), and (c) at 50 to 300 ma dc, (d) at 5 amp pulsed.

Fig. 8. B_c vs pressure R = 0.9 cm: Δ H_2, I = 200 ma; ▲ D_2, I = 200 ma; ■ D_2, I = 400 ma; —— H_2^+, I = 200 ma, theory of Kadomtsev and Nedospasov (K and N); —— D_2^+, I = 200 ma, theory of K and N; – – – – D_2^+, I = 400 ma theory of K and N; — – — He_2^+, theory of Hoh; —— – —— D_2^+, theory of Hoh.

Fig. 9. B_c vs pressure for R = 1.27 cm: Δ H_2, I = 200 ma; ▲ D_2, I = 200 ma; —— H_2^+, theory of K and N; —— D_2^+, theory of K and N; — – — H_2^+, theory of Hoh; —— – —— D_2^+, theory of Hoh.

Fig. 10. B_c vs pressure for R = 0.9 cm, He gas, I = 200 ma: —— theory of K and N, He^+ only; — – — theory of Hoh, He^+ only; —— – – —— theory of Hoh, He_2^+ only; —— — ——theory of K and N, He^+ only, $T_+ = 1000^\circ K$.

Fig. 11. B_c vs pressure for R = 1.27 cm: ▲ He, I = 200 ma; △ He, I = 400 ma; —— theory of K and N, 200 ma, He^+ only; – – – – theory of K and N, 400 ma, He^+ only; — – — theory of Hoh, He^+ only; — – – — theory of Hoh, He^+2 only.

Fig. 12. B_c vs pressure R = 2.75 cm, He gas: △ I =200 ma, and ▲ I = 500 ma, "long tube" system; O I = 200 ma, ● I = 400 ma, "short tube" system; —— theory of K and N, He^+ only; — – — theory of Hoh, He^+ only; — – – — theory of Hoh; He^+_2 only.

Fig. 13. B_c vs pressure for R = 0.9 cm, Ne gas, 200 ma: —— theory of K and N, Ne^+ only; — — — theory of K and N, Ne^+_2 only. — – — theory of Hoh, Ne^+ only; — – – — theory of Hoh, Ne^+_2 only.

Fig. 14. B_c vs pressure for R = 1.27 cm, Ne gas, △ 200 ma and ▲ 400 ma: —— theory of K and N, 200 ma, Ne^+ only; – – – – theory of K and N, 200 ma, Ne^+_2 only; — – — theory of Hoh, Ne^+ only; — – – — theory of Hoh, Ne^+_2 only.

Fig. 15. B_c vs pressure for R = 0.9 cm, A gas, 200 ma: —— theory of K and N, A^+ only; – – – – theory of K and N, A^+_2 only; — – — theory of Hoh, A^+ only; — – – — theory of Hoh, A^+_2 only.

Fig. 16. B_c vs pressure for R = 1.27 cm, A gas, 200 ma: —— theory of K and N, A^+ only; – – – theory of K and N, A^+_2 only; — – — theory of Hoh, A^+_2 only.

Fig. 17. Apparent electron temperature, as measured with Langmuir probe near tube center, vs B; R = 2.75 cm, p = 0.22 mm Hg, I = 200 ma, He gas. Dashed line is theoretical curve.

Fig. 18. 90-deg stereo streak photographs of helical constriction in He. Traces show variation of light intensity with time and radius as seen through a slit perpendicular to axis of discharge tube: (a) R = 2.75 cm, p = 0.23 mm Hg, B = 710 gauss, and (b) R = 0.9 cm, p = 0.5 mm Hg, B = 1990 gauss. Note that these are not photographs of helices; the helicity has been established by wavelength measurements with photomultipliers.

Fig. 19. Spiral wavelength λ vs pressure for R = 0.9 cm, I = 400 ma: Δ H_2 experimental, ——— H_2 theoretical ▲ D_2 experimental, — — — D_2 theoretical.

Fig. 20. Spiral wavelength λ vs pressure for R = 0.9 cm, I = 400 ma, He gas. Solid line is theoretical curve.

Fig. 21. Spiral wavelength λ vs pressure for R = 1.27 cm, I = 400 ma, He gas. Solid line is theoretical curve.

Fig. 22. Spiral wavelength λ vs pressure for R = 2.75 cm, He gas: ▲ 200 ma and Δ 400 ma. Solid line is theoretical curve.

Fig. 23. Spiral wavelength λ vs pressure for R = 1.27 cm, Ne gas, I = 200 ma. Solid line is theoretical curve.

Fig. 24. Spiral wavelength λ vs length of magnet coil for R = 2.75 cm, He gas: Δ p = 0.11 mm Hg, 400 ma; O p = 0.17 mm Hg, 400 ma; ■ p = 0.27 mm Hg, 200 ma; □ p = 0.27 mm Hg, 400 ma.

Fig. 25. Pitch and direction of rotation of helix as a function of the direction of the magnetic field.

Fig. 26. Ion current distribution (μa) across tube as collected by negative probe; R = 2.75 cm, He gas, p = 0.23 mm Hg, I = 300 ma, B = 767 gauss.

Fig. 27. Frequency of rotation of luminous channel, ω_r, vs pressure for R = 0.9 cm, I = 400 ma: Δ H_2 experimental, —— H_2 theoretical, ▲ D_2 experimental, —— – —— D_2 theoretical.

Fig. 28. Frequency of rotation of luminous channel, ω_r, vs pressure for R = 1.27 cm, I = 400 ma: Δ H_2 experimental, —— H_2 theoretical, ▲ D_2 experimental, —— – —— D_2 theoretical.

Fig. 29. Frequency of rotation of luminous channel, ω_r, vs pressure for R = 0.9 cm, He gas, I = 400 ma. Solid line is theoretical curve.

Fig. 30. Frequency of rotation of luminous channel, ω_r, vs pressure for R = 1.27 cm, He gas, I = 400 ma. Solid line is theoretical curve.

Fig. 31. Frequency of rotation of luminous channel, ω_r, bs pressure for R = 2.75 cm, He gas: Δ 400 ma and ▲ 200 ma. Solid line is theoretical curve.

Fig. 32. Frequency of rotation of luminous channel, ω_r, vs pressure for R = 1.27 cm, I = 200 ma, Ne gas. Solid line is theoretical curve.

Fig. 33. 90-deg stereo streak photographs. Traces show variation of light intensity with time and radius, in helium discharges: (a) R = 2.75 cm, p = 0.23 mm Hg, B = 979 gauss; and (b) R = 0.9 cm, p = 0.2 mm Hg, B = 994 gauss < B_c (moving striations).

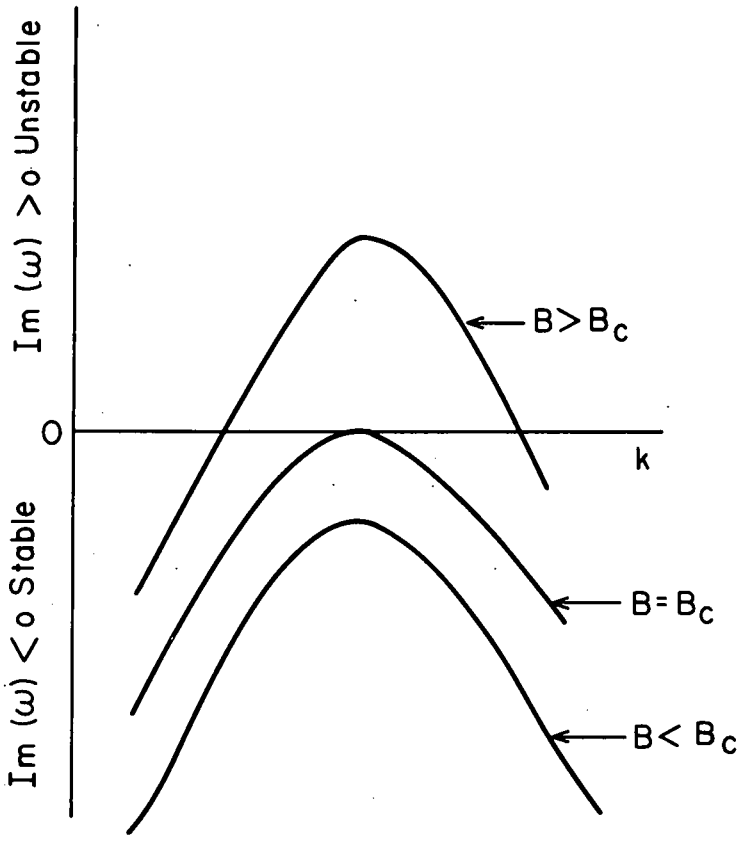

Fig. 1

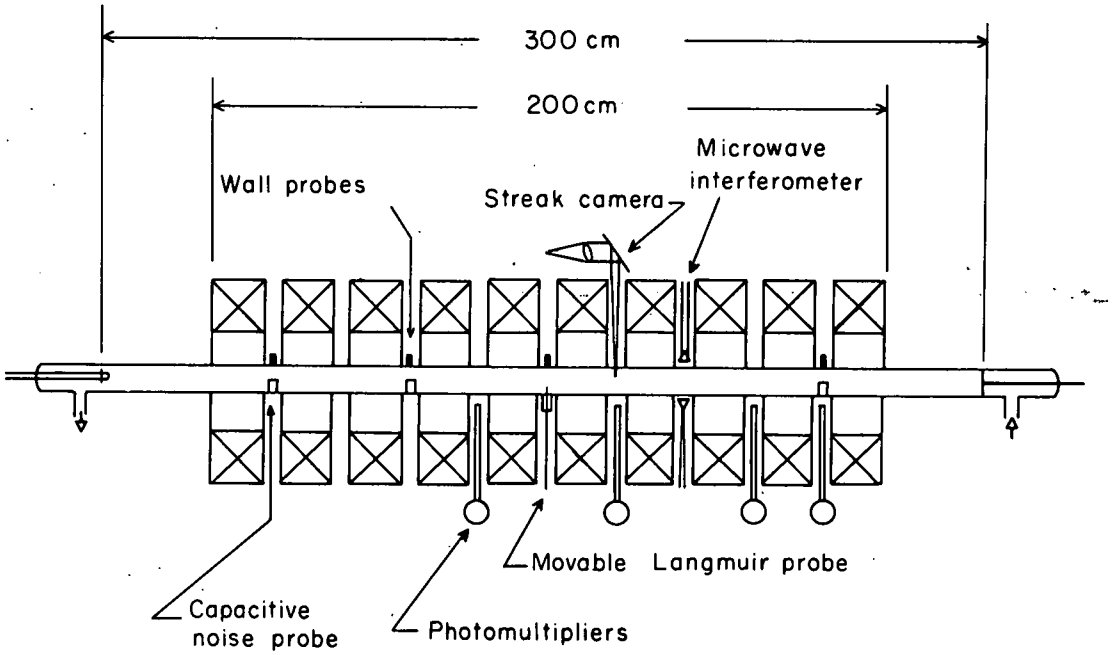
300 cm
200 cm
Wall probes
Streak camera
Microwave interferometer
Capacitive noise probe
Photomultipliers
Movable Langmuir probe
MU-20590

Fig. 2

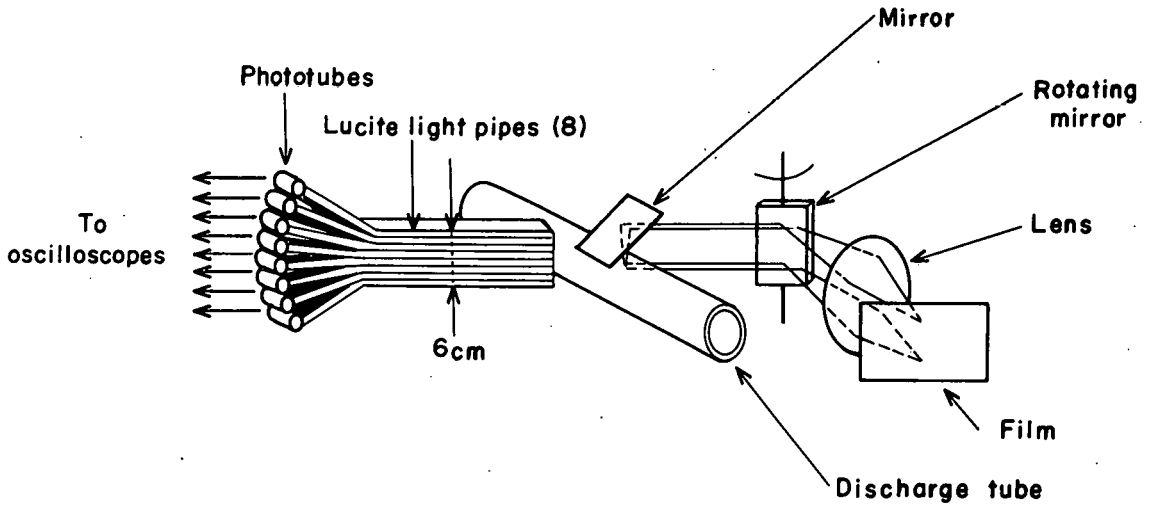
Photomultiplier Bank
Streak Camera
Mirror
Phototubes
Rotating mirror
Lucite light pipes (8)
To oscilloscopes
Lens
6cm
Film
Discharge tube
MU-22933

Fig. 3

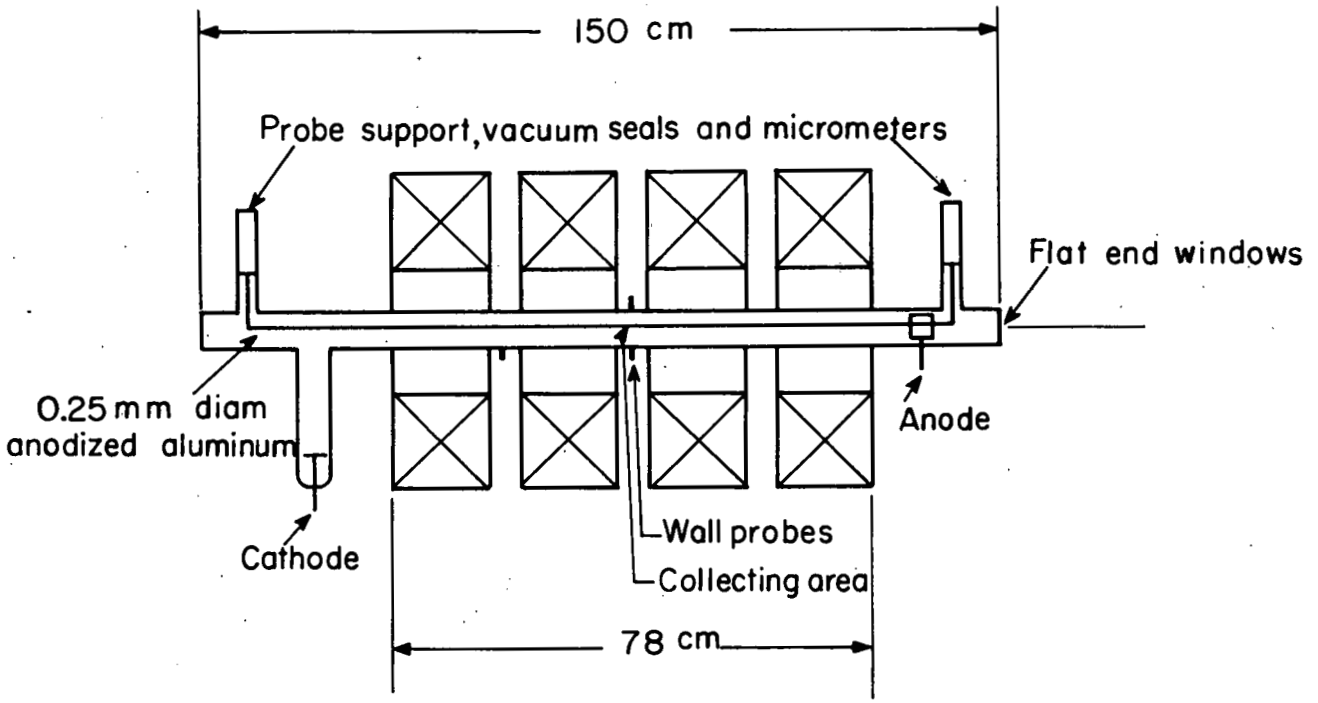
150 cm
Probe support, vacuum seals and micrometers
Flat end windows
0.25 mm diam
anodized aluminum
Anode
Cathode
Wall probes
Collecting area
78 cm
MU-22939

Fig. 4

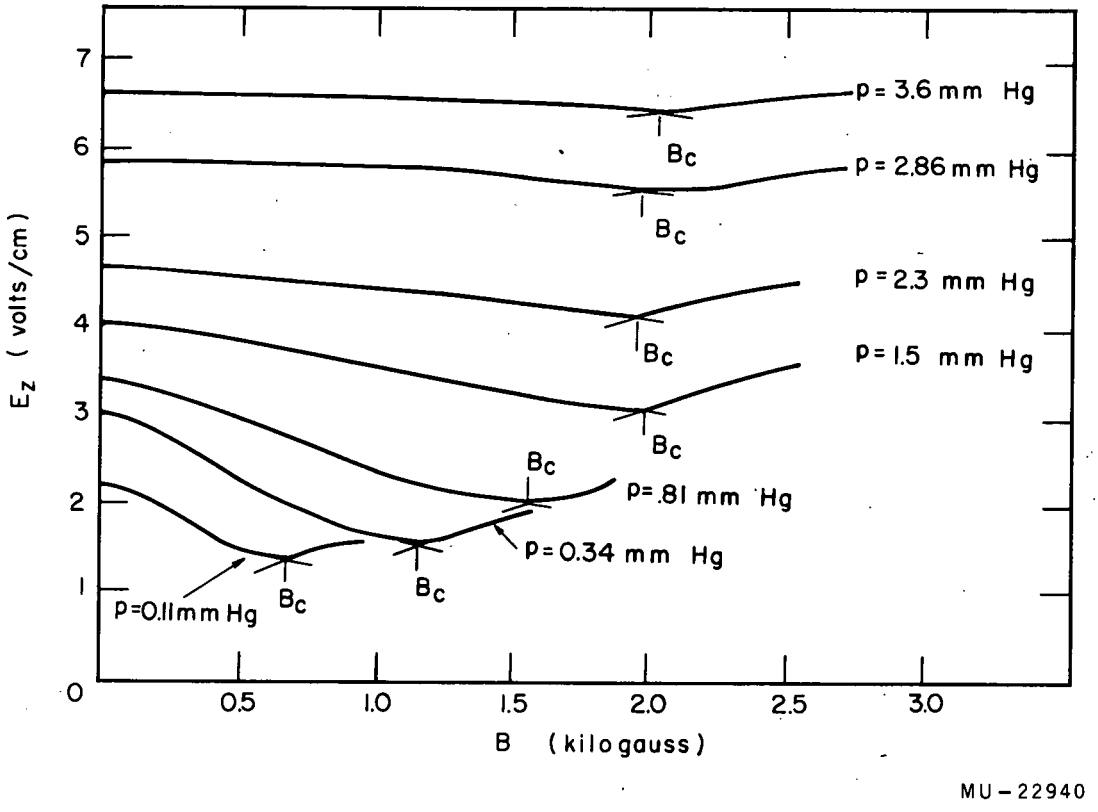
p = 3.6 mm Hg
p = 2.86 mm Hg
p = 2.3 mm Hg
p = 1.5 mm Hg
p = .81 mm Hg
p = 0.34 mm Hg
p = 0.11 mm Hg
Bc
E_z (volts/cm)
B (kilogauss)
0
1
2
3
4
5
6
7
0.5
1.0
1.5
2.0
2.5
3.0
MU-22940

Fig. 5

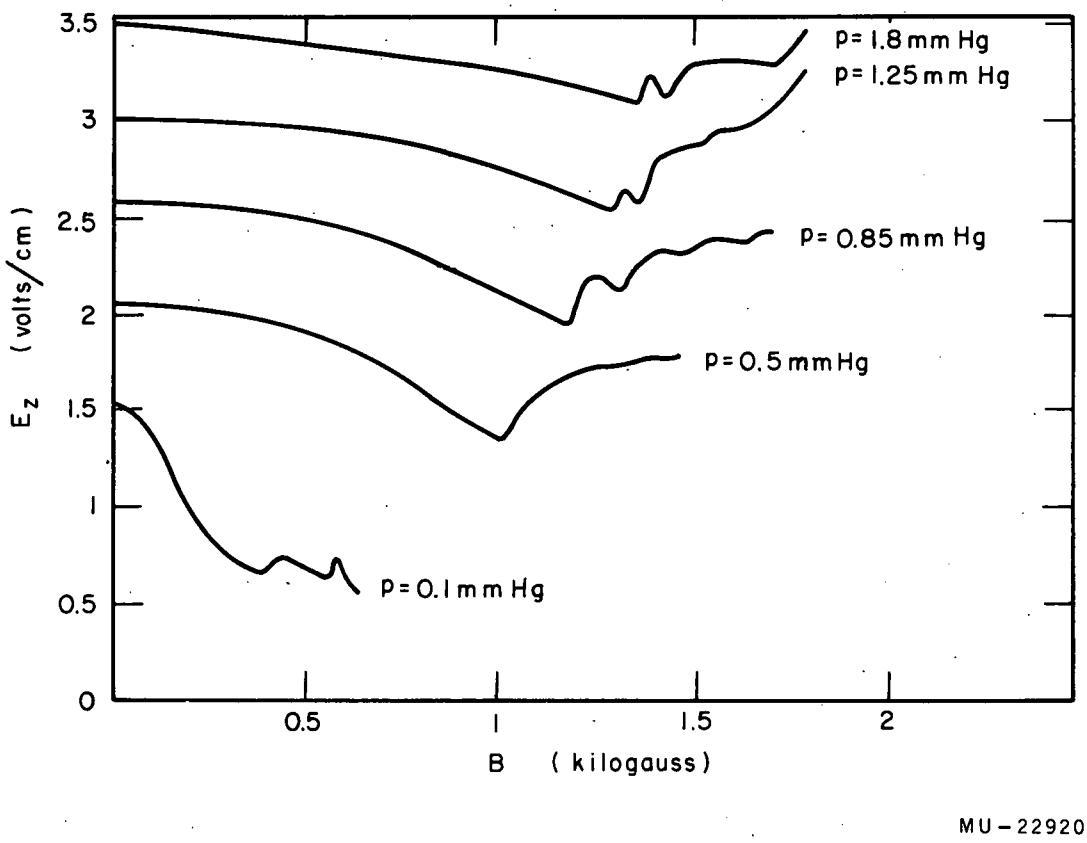
3.5
3
2.5
2
1.5
1
0.5
0
E_z (volts/cm)
p= 1.8 mm Hg
p= 1.25 mm Hg
p= 0.85 mm Hg
p= 0.5 mm Hg
p= 0.1 mm Hg
0.5
1
1.5
2
B (kilogauss)
MU-22920

Fig. 6

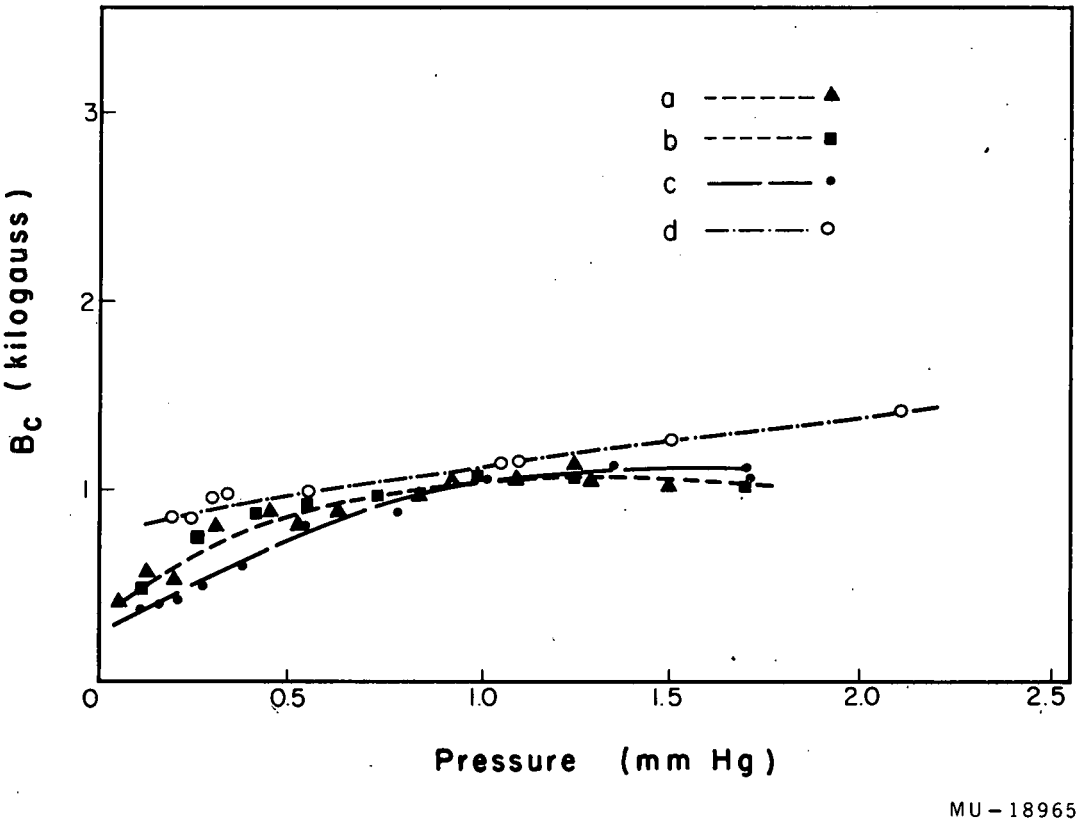

Fig. 7

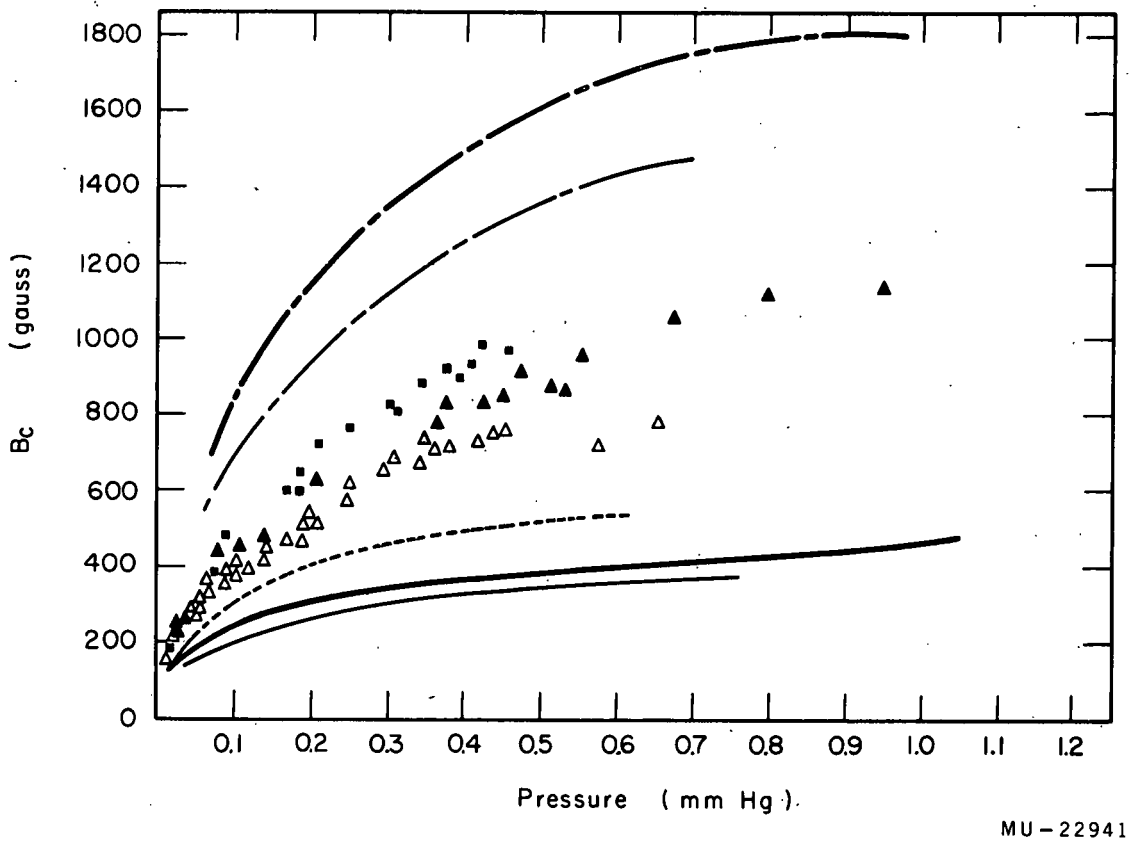
1800
1600
1400
1200
1000
800
600
400
200
0
B_c (gauss)
0.1
0.2
0.3
0.4
0.5
0.6
0.7
0.8
0.9
1.0
1.1
1.2
Pressure (mm Hg)
MU-22941

Fig. 8

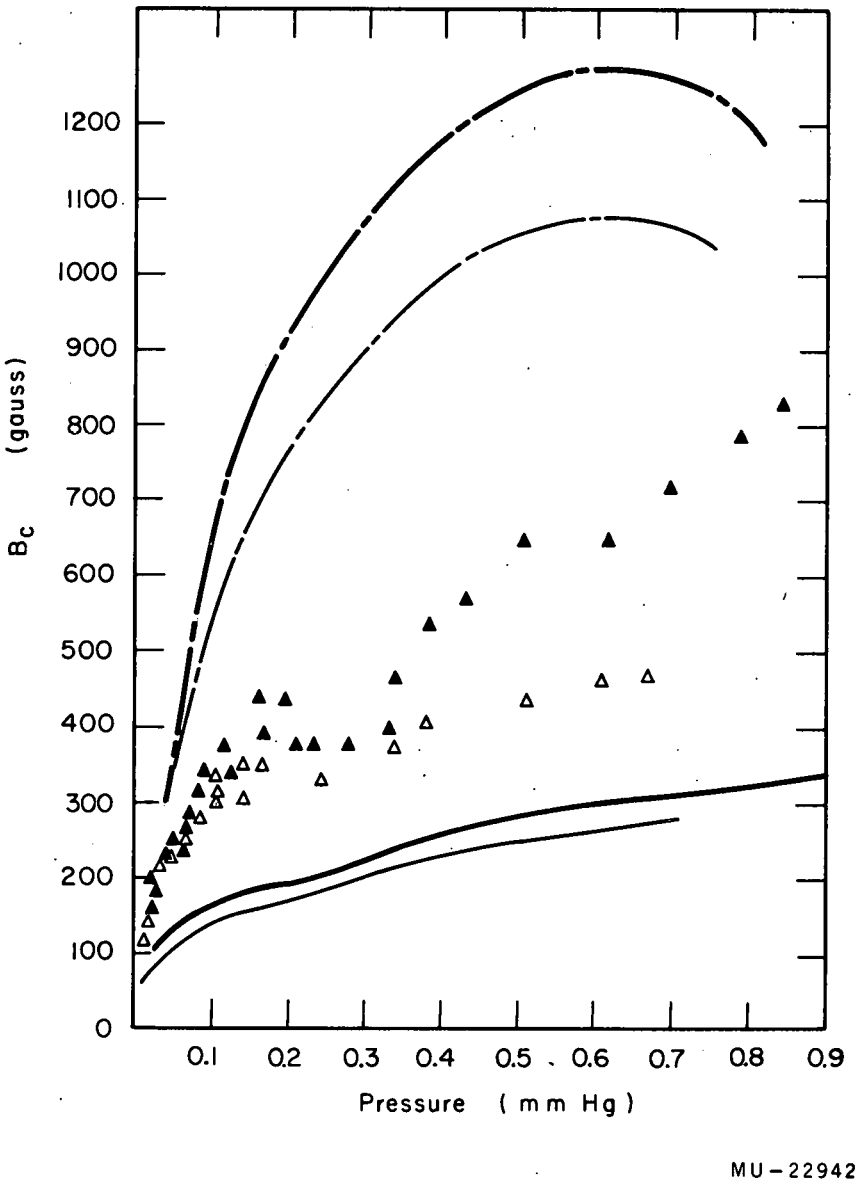
1200
1100
1000
900
800
700
600
500
400
300
200
100
0
B_c (gauss)
0.1
0.2
0.3
0.4
0.5
0.6
0.7
0.8
0.9
Pressure (mm Hg)
MU-22942

Fig. 9

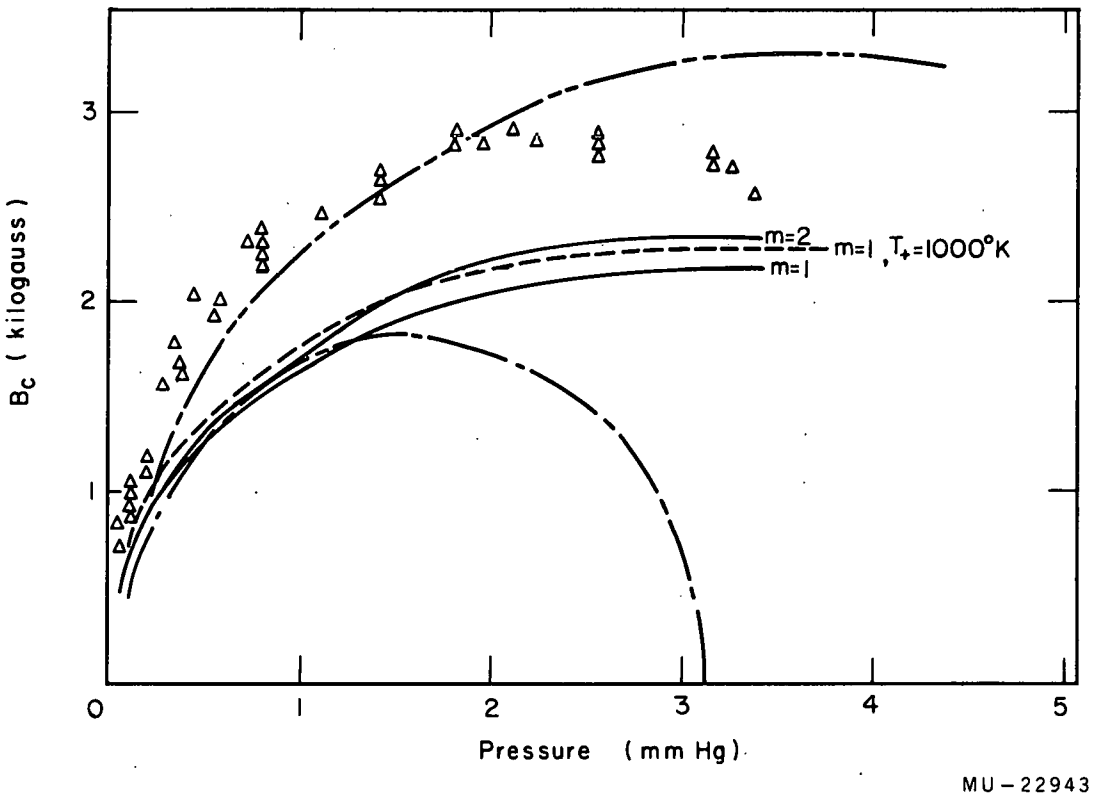
B_c (kilogauss)
3
2
1
0
1
2
3
4
5
Pressure (mm Hg)
m=2
m=1
m=1
T_+=1000°K
MU-22943

Fig. 10

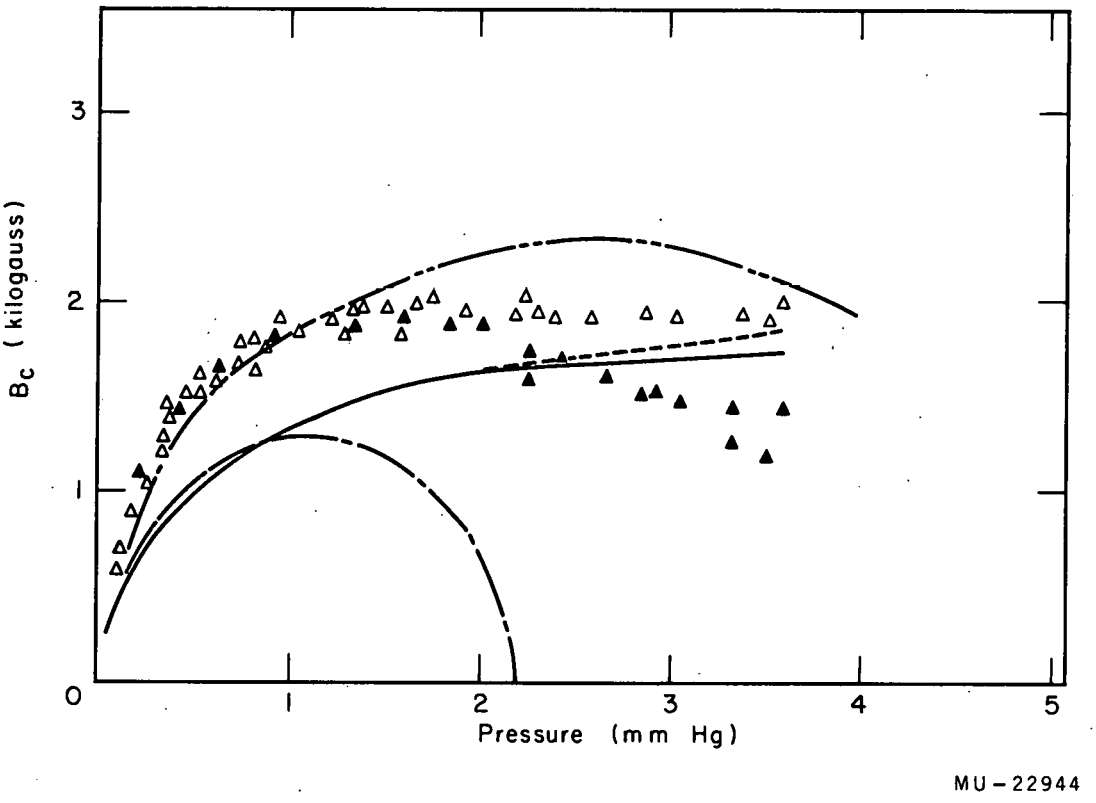

Fig. 11

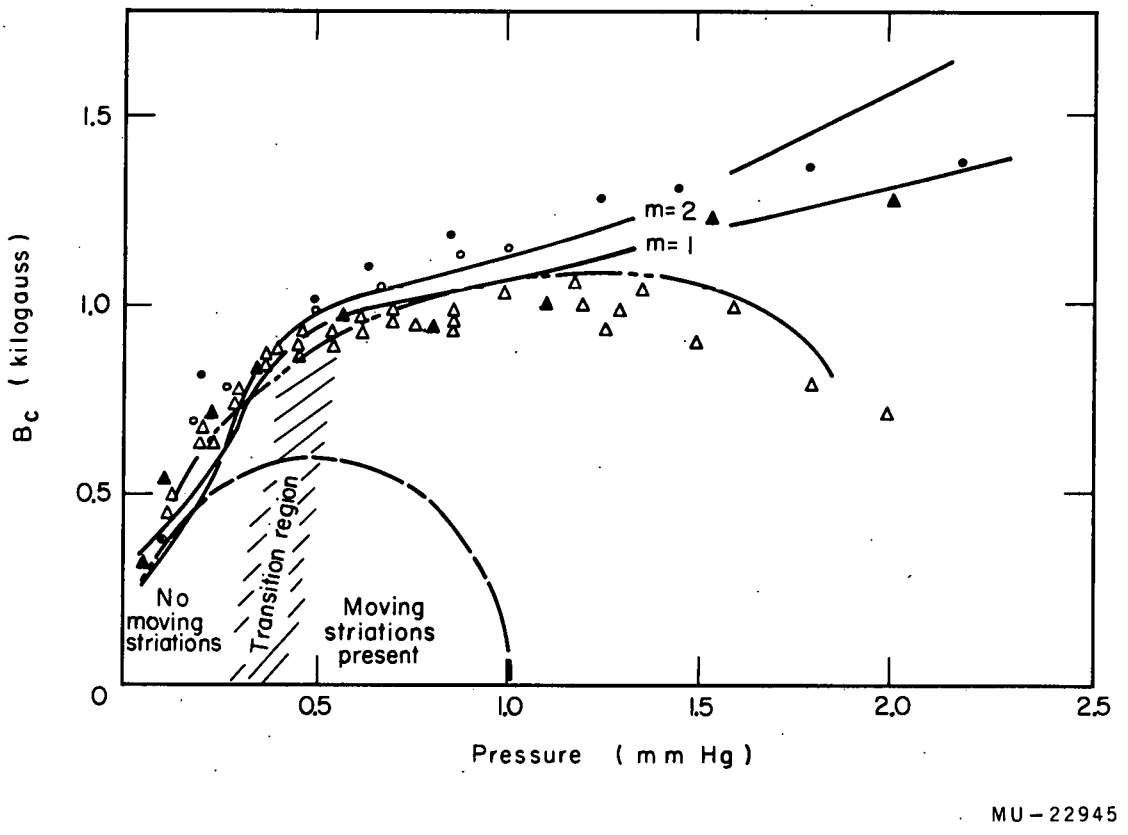
1.5
1.0
0.5
0
B_c (kilogauss)
m= 2
m= 1
No moving striations
Transition region
Moving striations present
0.5
1.0
1.5
2.0
2.5
Pressure (mm Hg)
MU-22945

Fig. 12

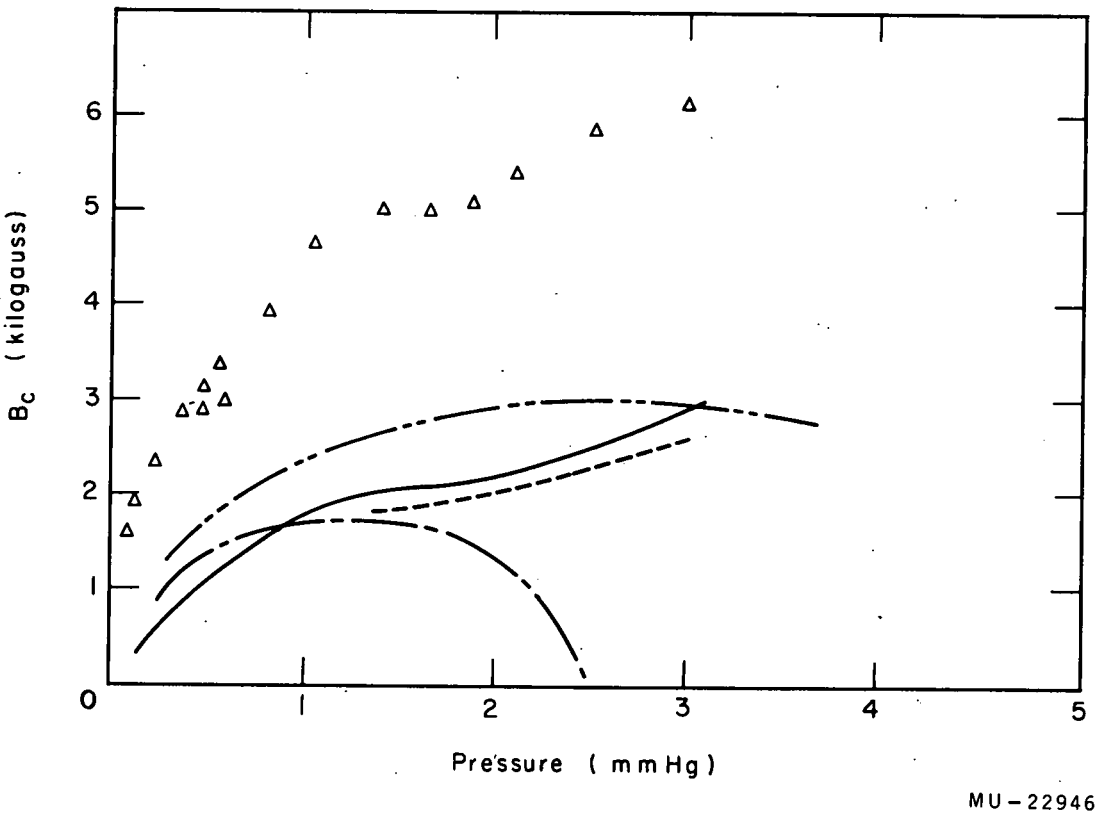

Fig. 13

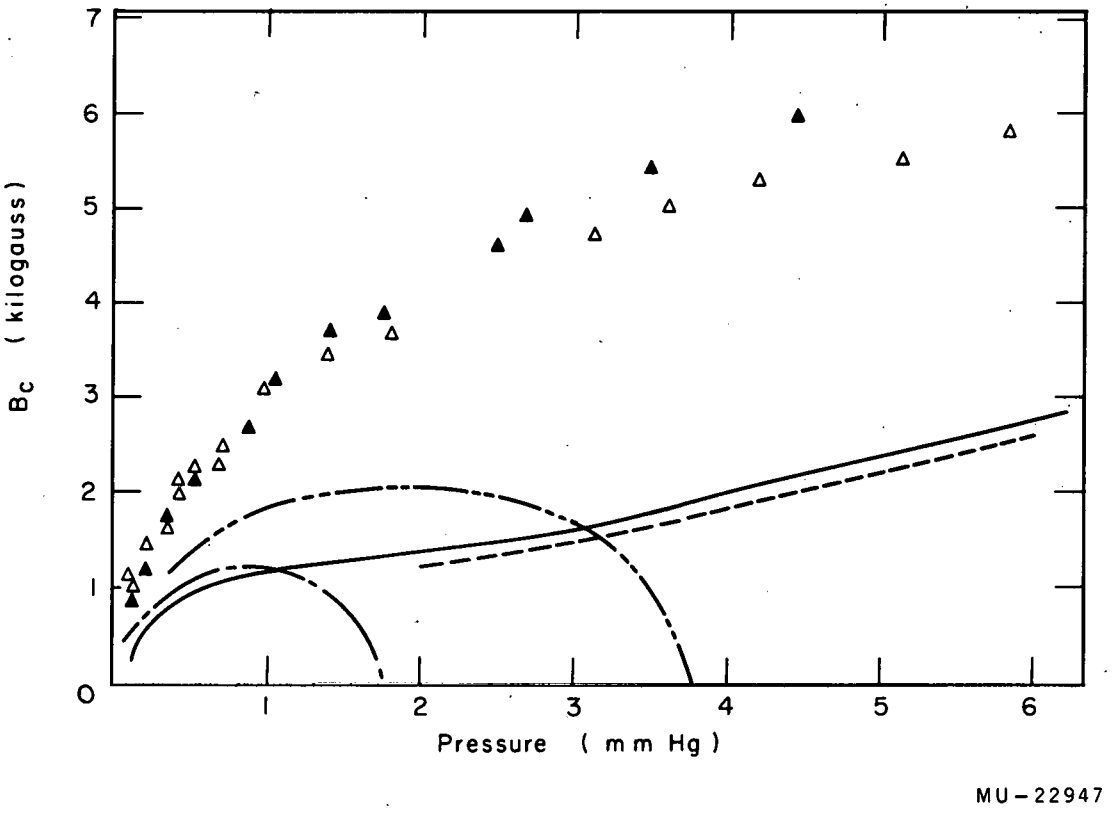

Fig. 14

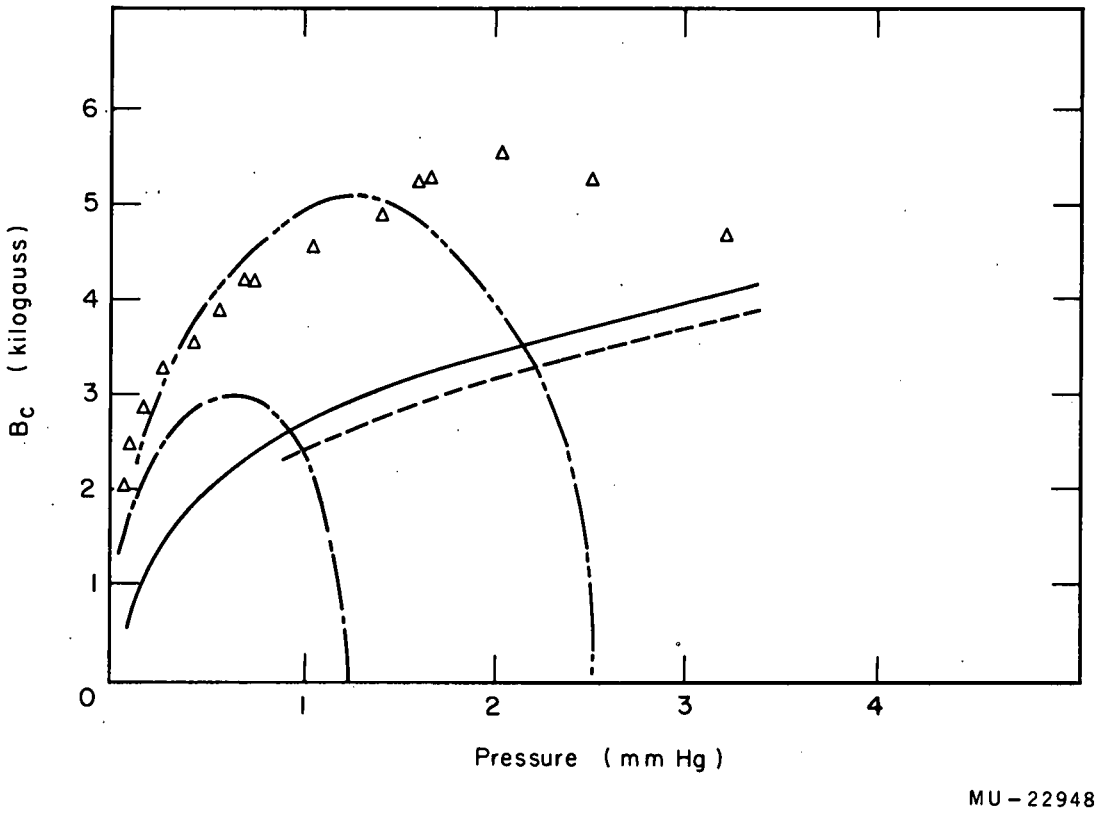

Fig. 15

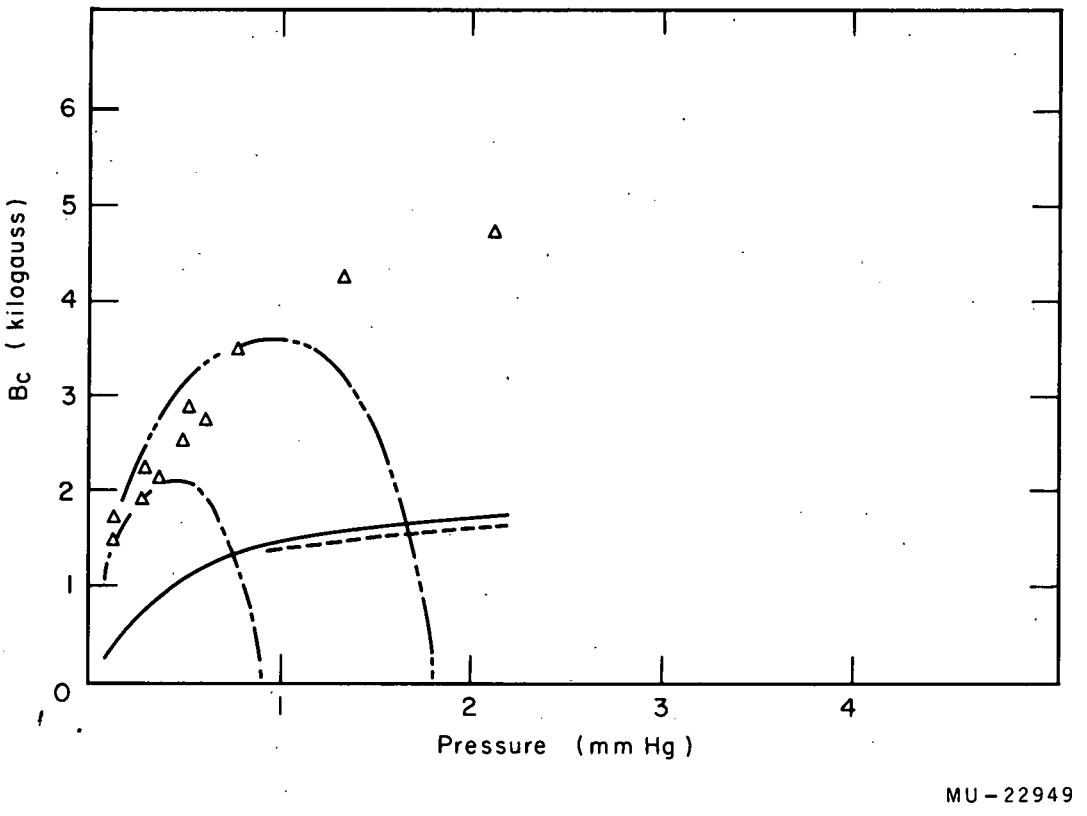

Fig. 16

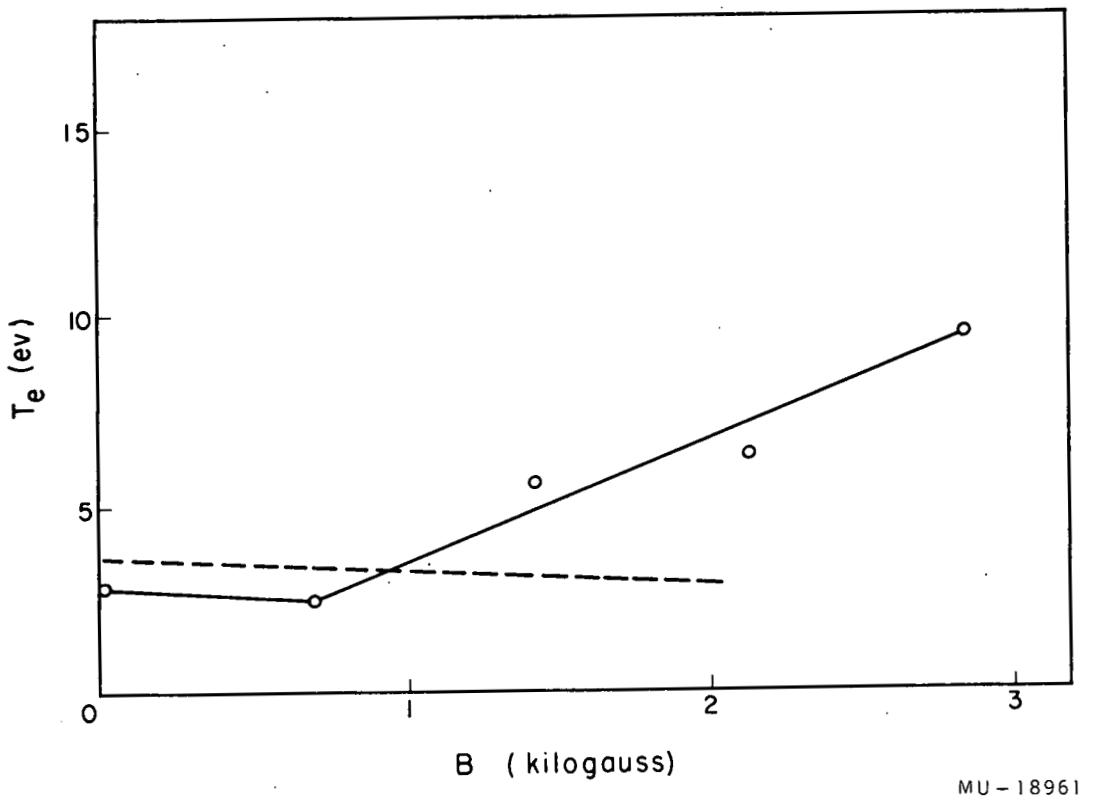

Fig. 17

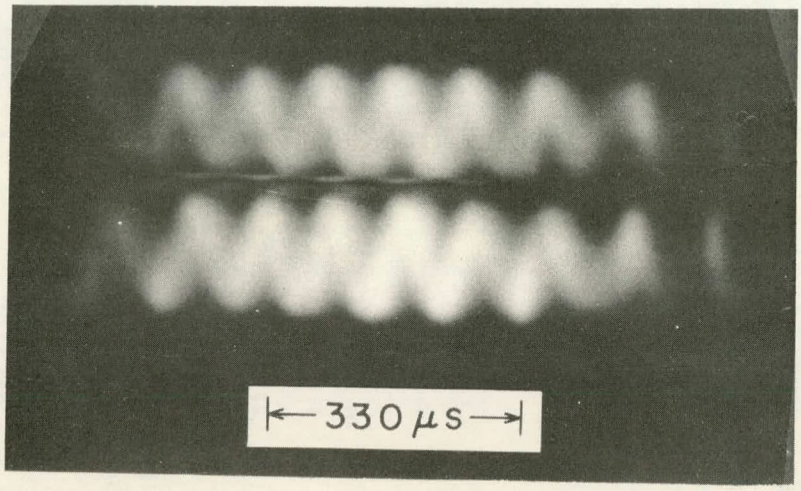

(a)

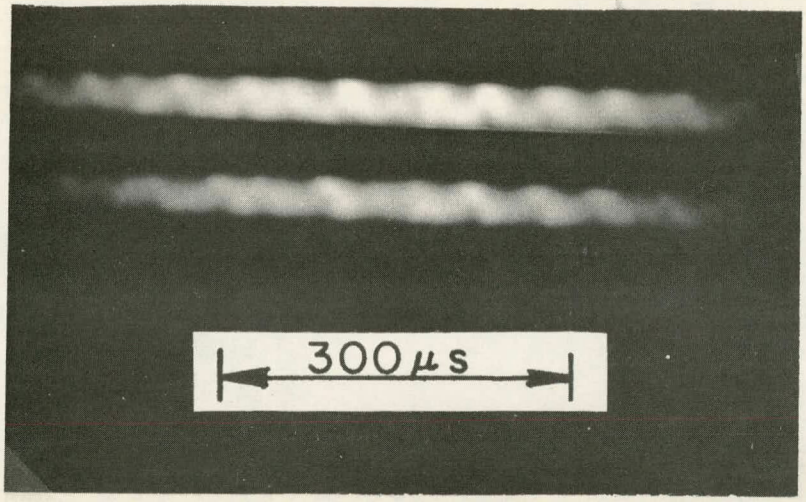

(b)

ZN-2714

Fig. 18

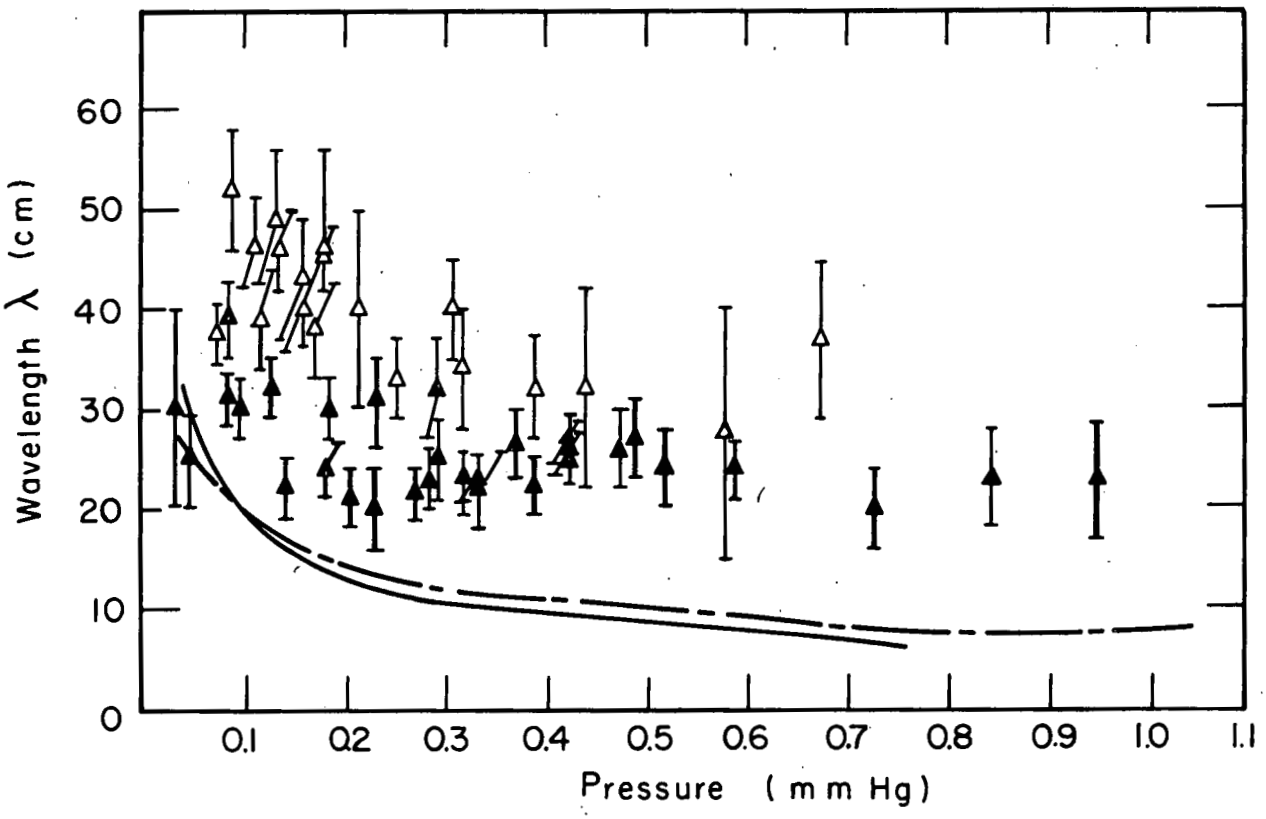
Wavelength λ (cm)
60
50
40
30
20
10
0
0.1
0.2
0.3
0.4
0.5
0.6
0.7
0.8
0.9
1.0
1.1
Pressure (mm Hg)
MU-22950

Fig. 19

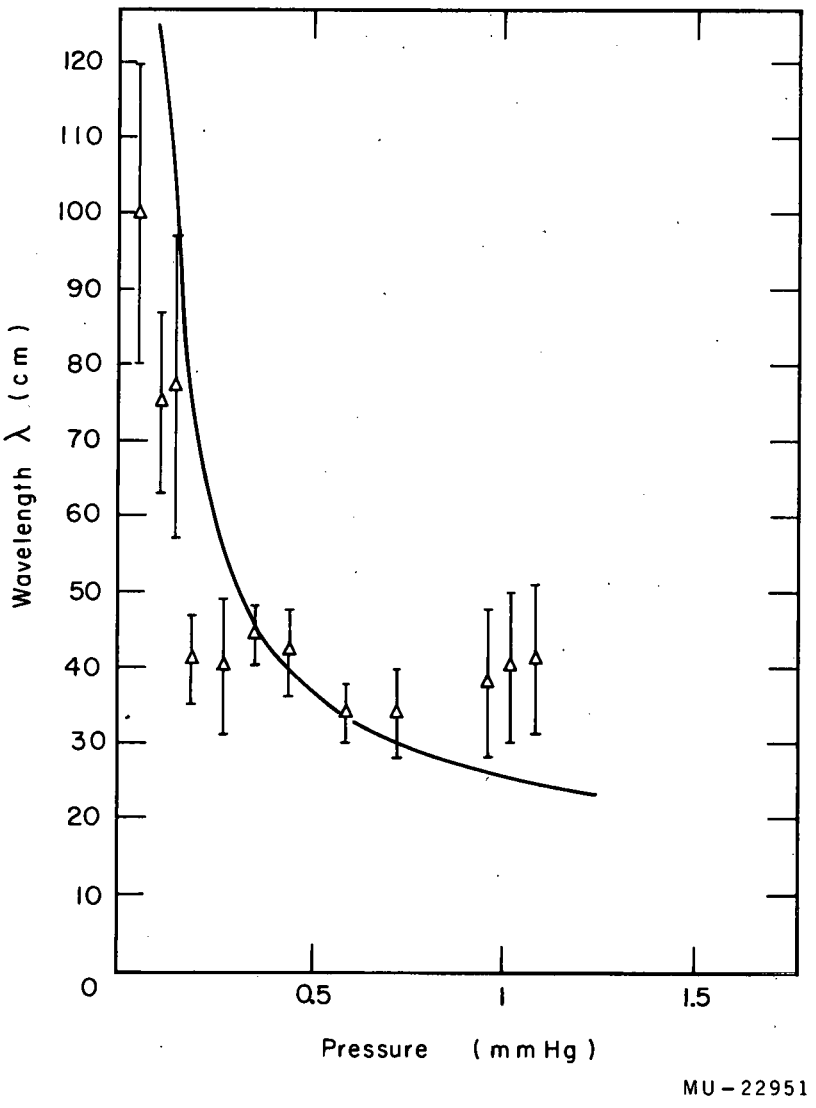
120
110
100
90
80
70
60
50
40
30
20
10
0
Wavelength λ (cm)
0.5
1
1.5
Pressure (mm Hg)
MU-22951

Fig. 20

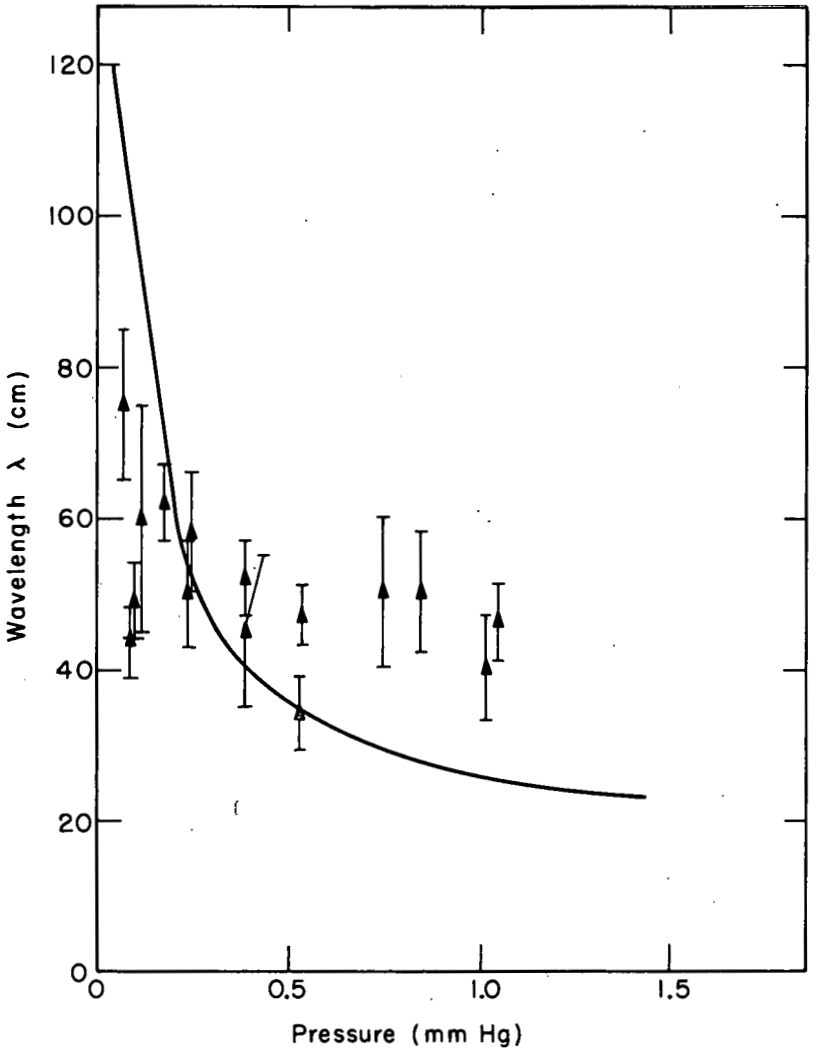
120
100
80
60
40
20
0
0
0.5
1.0
1.5
Wavelength λ (cm)
Pressure (mm Hg)
MU-22579

Fig. 21

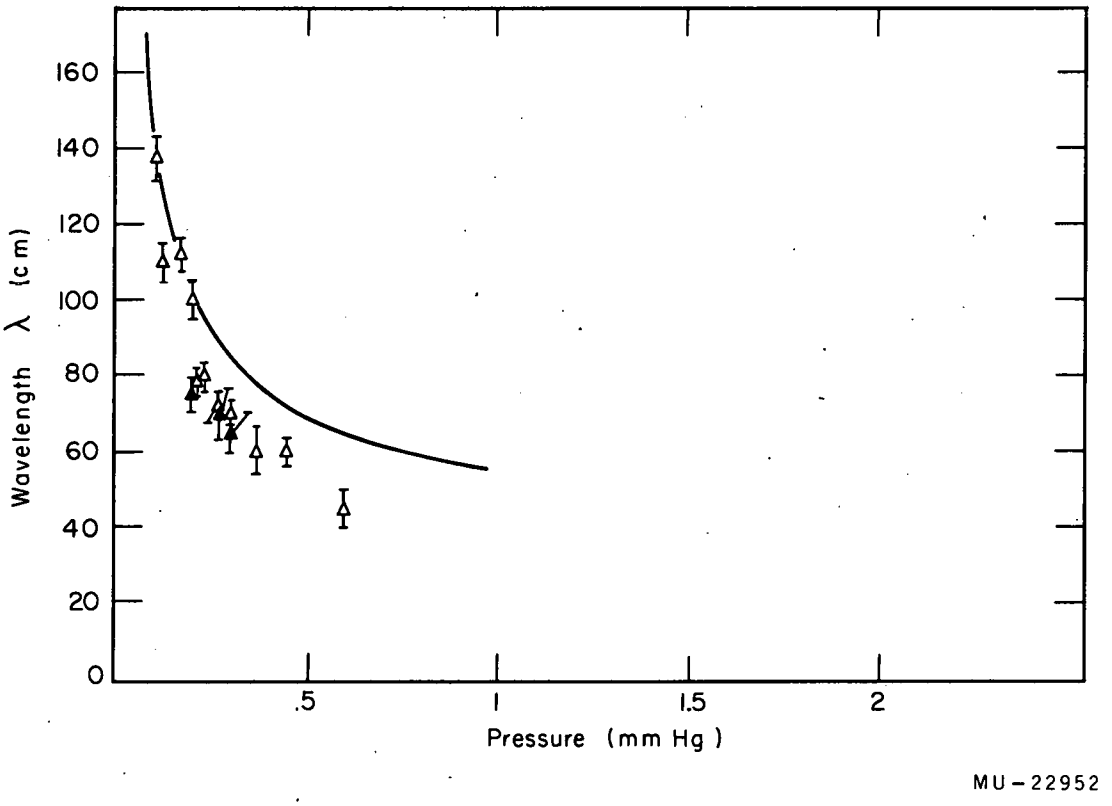
160
140
120
100
80
60
40
20
0
Wavelength λ (cm)
.5
1
1.5
2
Pressure (mm Hg)
MU-22952

Fig. 22

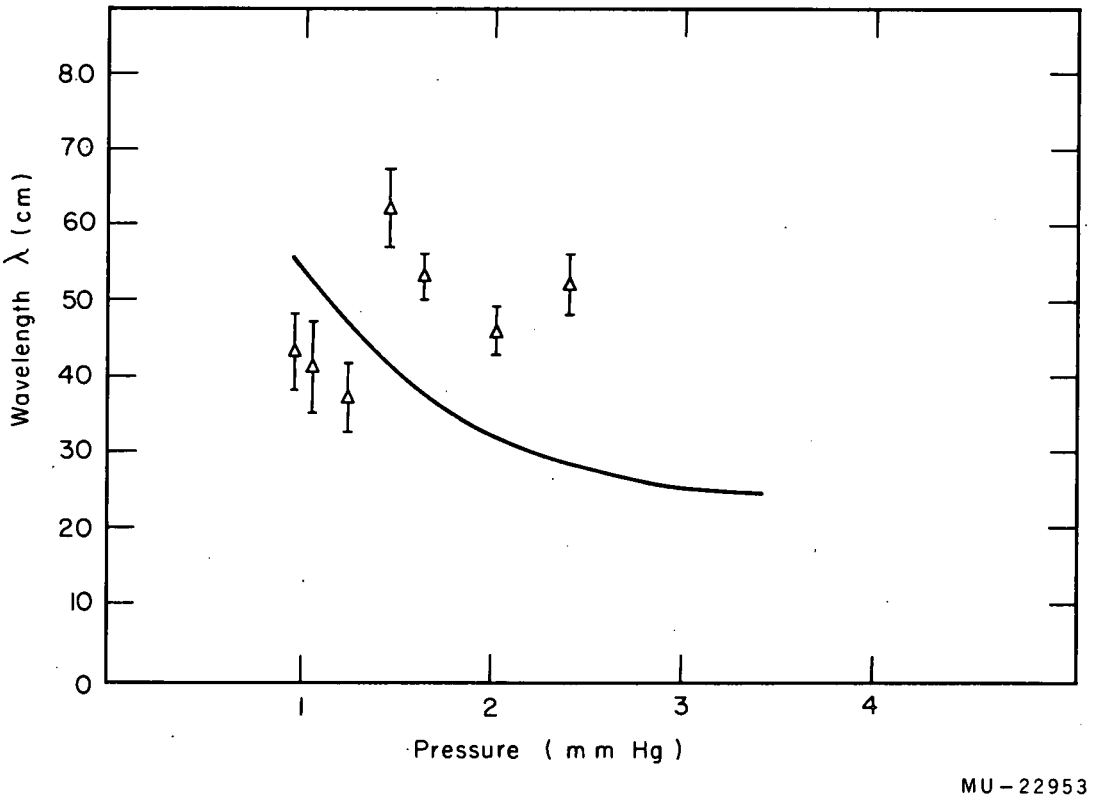
Wavelength λ (cm)
80
70
60
50
40
30
20
10
0
1
2
3
4
Pressure (m m Hg)
MU-22953

Fig. 23

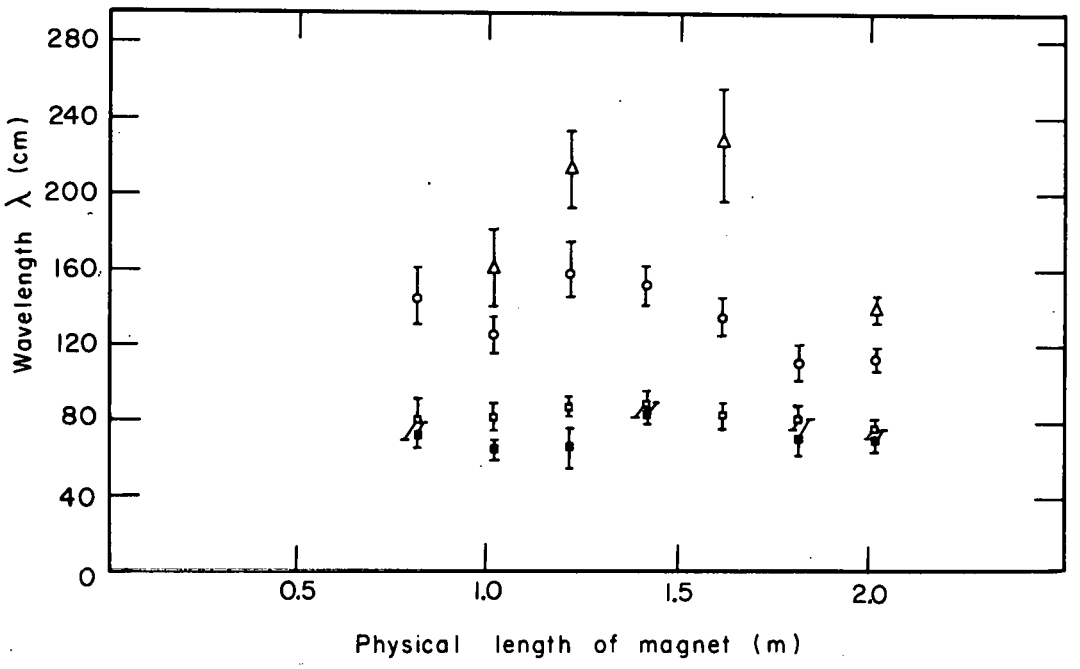
Wavelength λ (cm)
280
240
200
160
120
80
40
0
0.5
1.0
1.5
2.0
Physical length of magnet (m)
MU-22954

Fig. 24

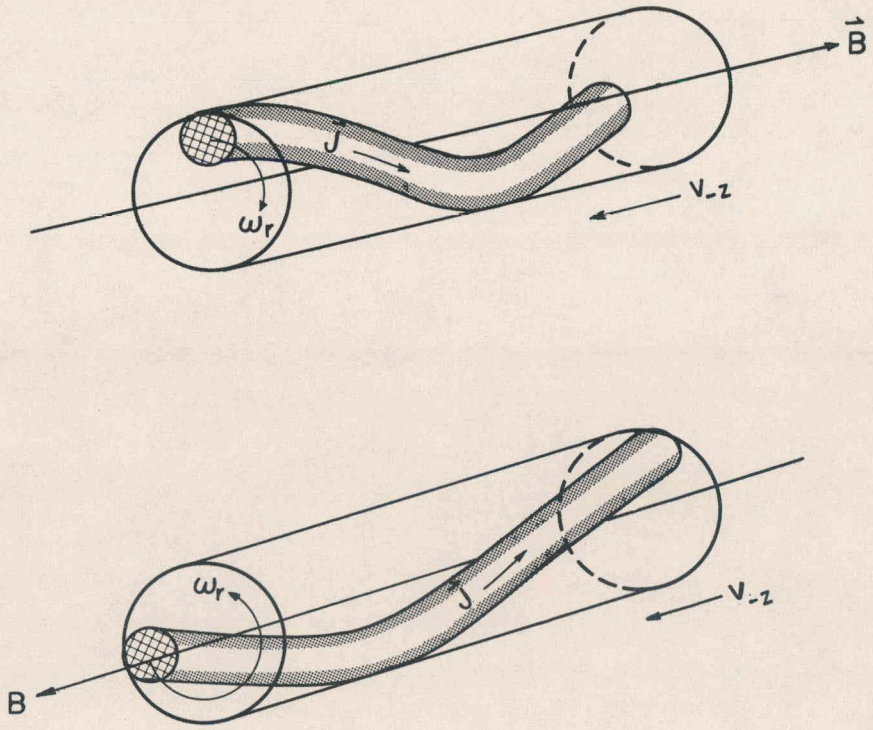

MU-22956

Fig. 25

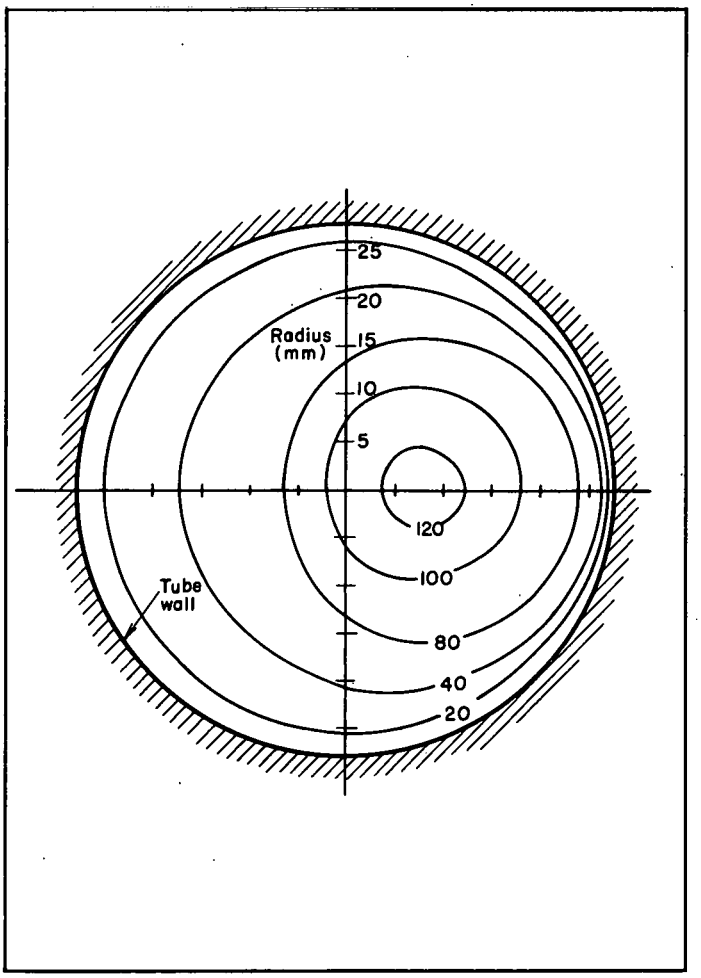

MU-22957

Fig. 26

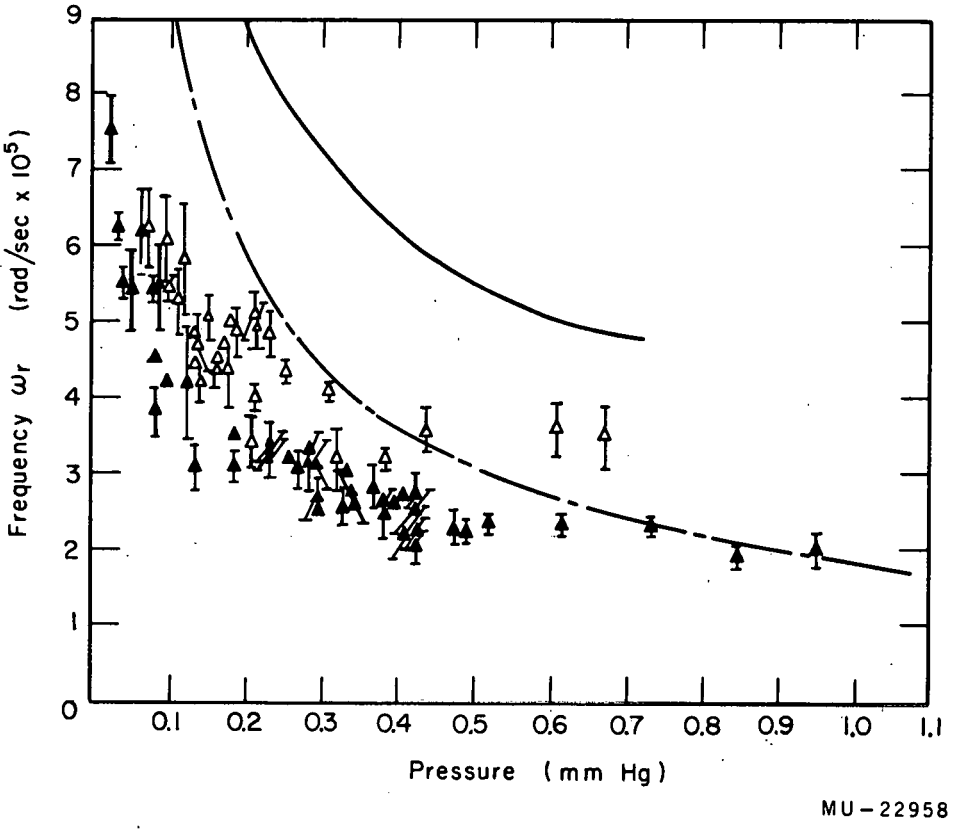
Frequency ω_r (rad/sec x 10^5)
9
8
7
6
5
4
3
2
1
0
0.1
0.2
0.3
0.4
0.5
0.6
0.7
0.8
0.9
1.0
1.1
Pressure (mm Hg)
MU-22958

Fig. 27

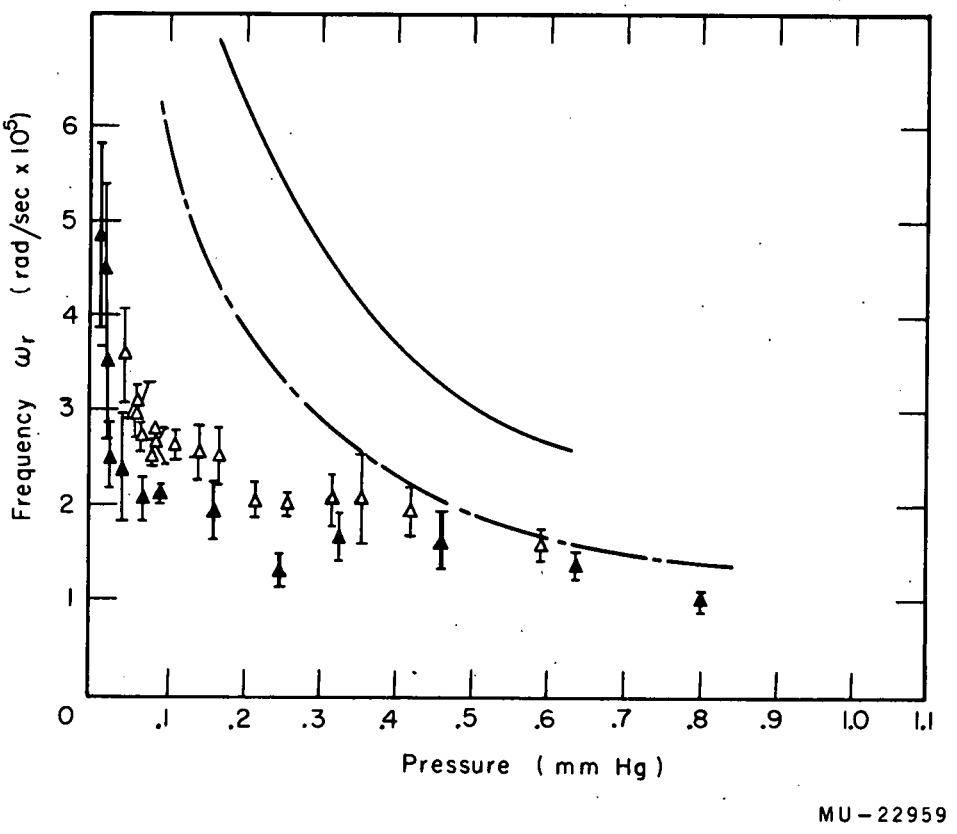
Frequency ω_r (rad/sec x 10^5)
0
1
2
3
4
5
6
.1
.2
.3
.4
.5
.6
.7
.8
.9
1.0
1.1
Pressure (mm Hg)
MU-22959

Fig. 28

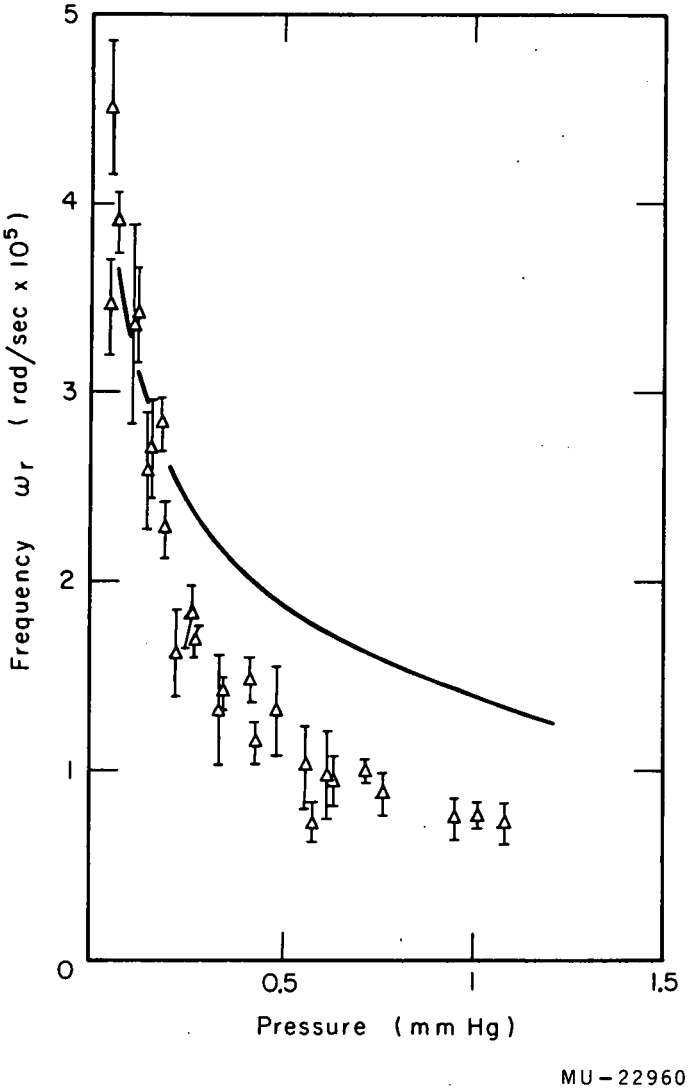
5
4
3
2
1
0
Frequency ω_r (rad/sec x 10^5)
0.5
1
1.5
Pressure (mm Hg)
MU-22960

Fig. 29

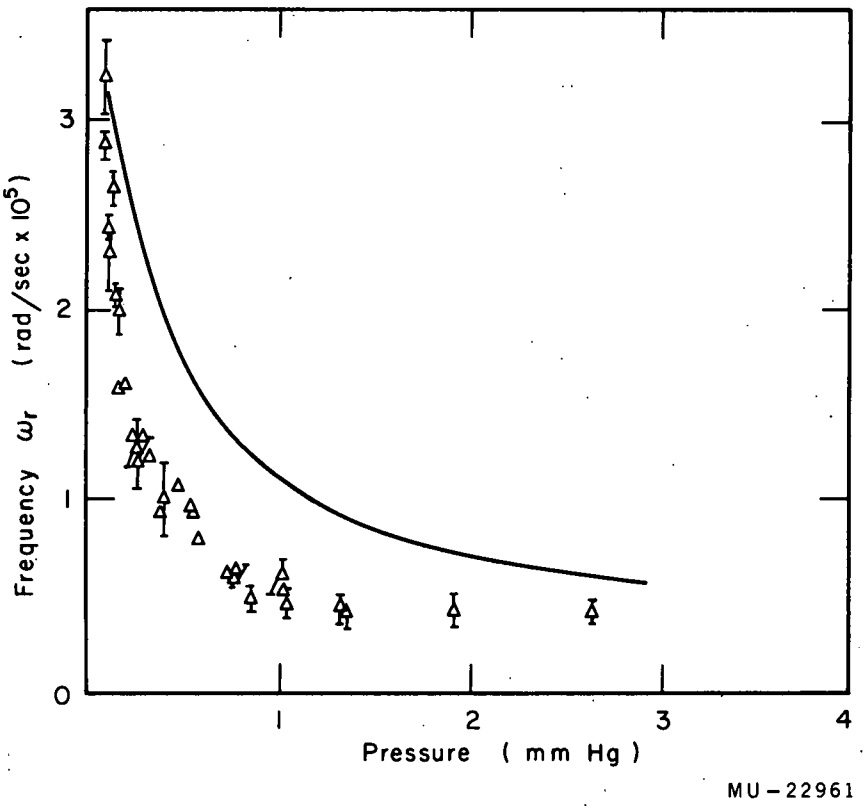
Frequency ω_r (rad/sec x 10^5)
3
2
1
0
1
2
3
4
Pressure (mm Hg)
MU-22961

Fig. 30

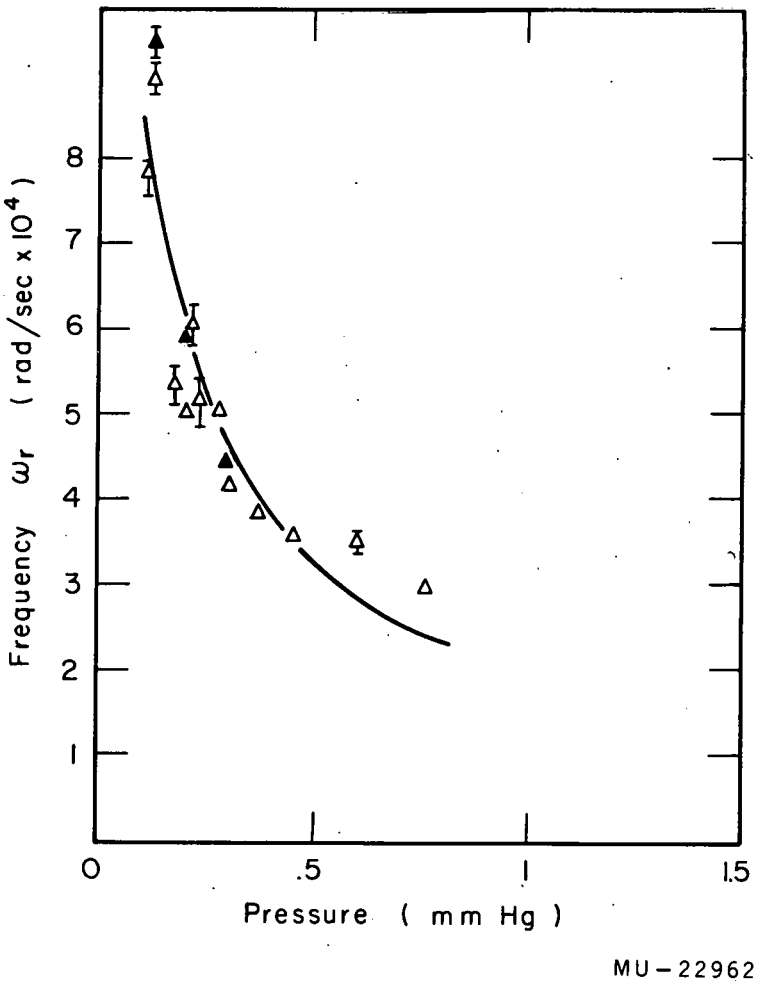
Frequency ω_r (rad/sec x 10^4)
8
7
6
5
4
3
2
1
0
.5
1
1.5
Pressure (mm Hg)
MU-22962

Fig. 31

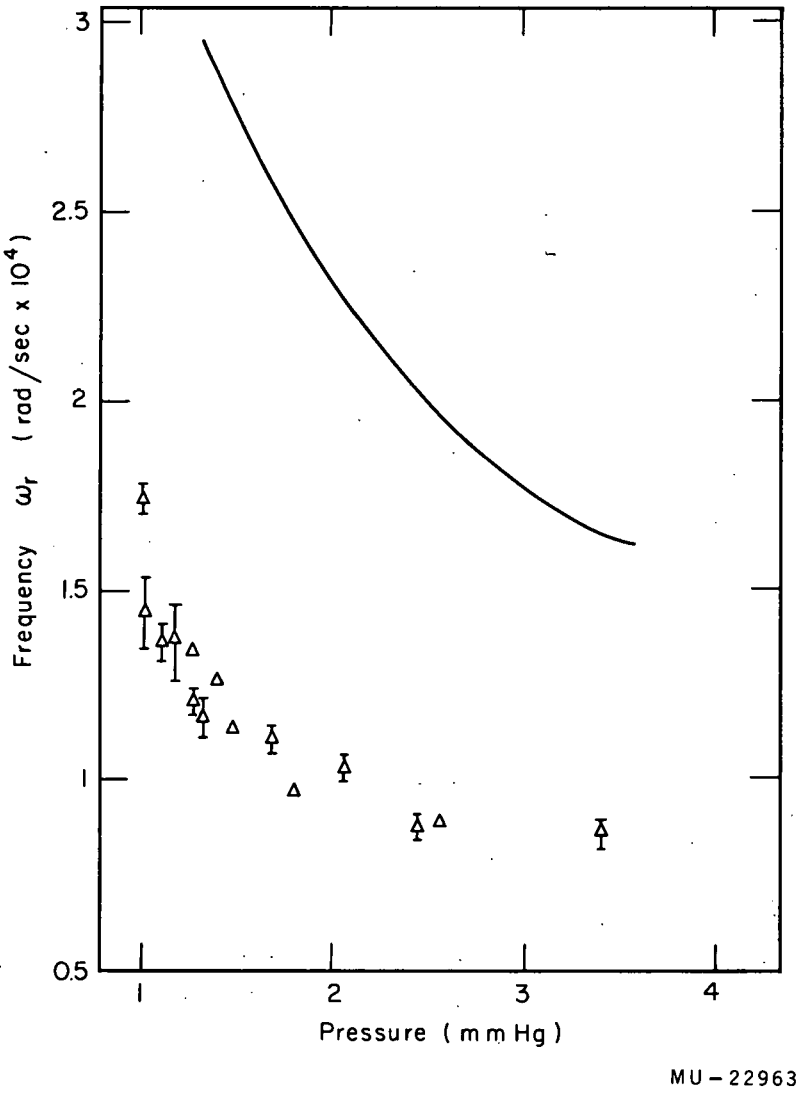
3
2.5
2
1.5
1
0.5
Frequency ω_r (rad/sec x 10^4)
1
2
3
4
Pressure (mm Hg)
MU-22963

Fig. 32

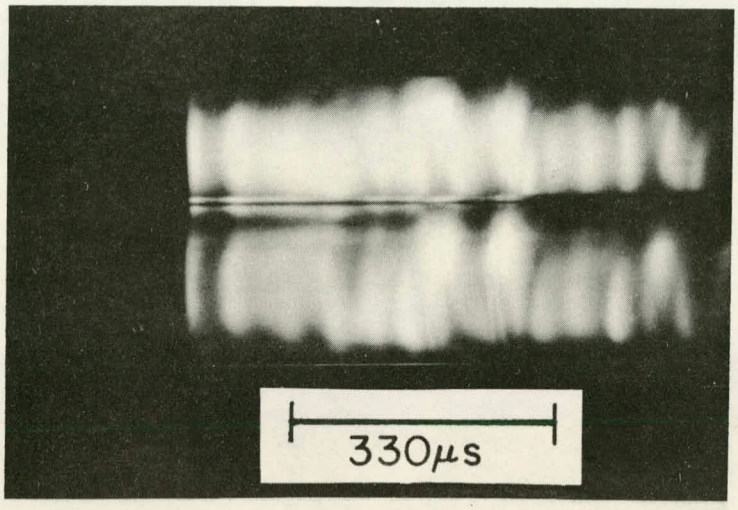

(a)

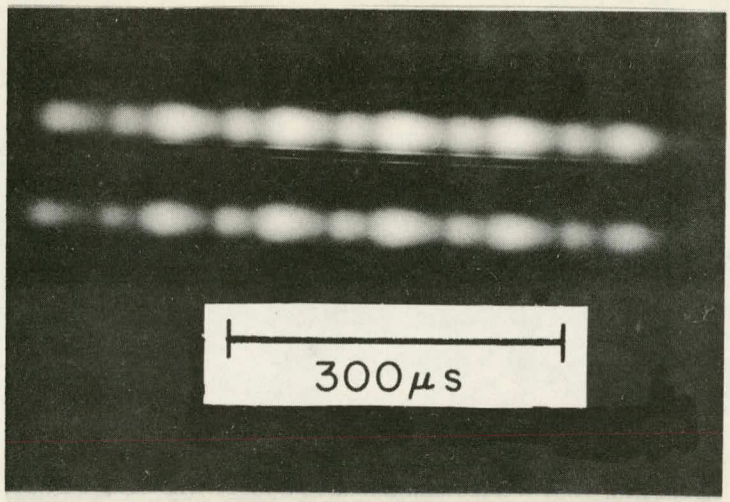

(b)

ZN-2713

Fig. 33